Revision 1

1 **Zeolite-group minerals in phonolite-hosted deposits of the Kaiserstuhl Volcanic Complex,**

2 **Germany**

3

4

5

6 [1][*]Simon Spürgin

7 [2]Tobias Björn Weisenberger

8 [3]Marija Marković
9

10 [1]Hans G. Hauri KG Mineralstoffwerke, Bergstr. 114, 79268 Bötzingen, Germany,

11 spuerg@gmx.de

12 [2] ÌSOR Iceland GeoSurvey, Grensásvegur 9, 108 Reykjavik, Iceland,

13 tobias.b.weisenberger@isor.is

14 [3]Institute for Technology of Nuclear and Other Mineral Raw Materials (ITNMS), Franshe d'

15 Epere 86, 11000 Belgrade, Serbia, m.markovic@itnms.ac.rs

16

17 [*] corresponding author

18

19

20 *American Mineralogist*

21

22

23

1

Revision 1

Abstract

24

25 Subvolcanic phonolite intrusions of the Kaiserstuhl Volcanic Complex (Germany) show

26 variable degrees of alteration. Their secondary mineralogy has been characterized by

27 petrographic textural observations, bulk-rock powder X-ray diffraction, thermogravimetry,

28 differential thermal analysis, and electron probe microanalysis. The alteration assemblage is

29 dominated by various zeolites that occur in fissures, vugs and as replacement products of

30 primary phases within the phonolite matrix. Phonolites in the eastern Kaiserstuhl were

31 emplaced into a sedimentary sequence and are characterized by high zeolite contents

32 (Endhalden: 48 wt%, Fohberg: 45 wt%) with the temporal sequence ±thomsonite-Ca –

33 ±mesolite – gonnardite – natrolite – analcime. In the western Kaiserstuhl zeolite contents

34 are lower (Kirchberg: 26 wt% or less) and the crystallization sequence is ±thomsonite-Ca –

35 gonnardite – natrolite – chabazite-Ca. Pseudomorphic replacement textures and barite

36 inclusions in secondary aggregates suggest that zeolites grew at the expense of a sulphate-

37 bearing sodalite-group mineral, i.e. haüyne. Fresh grains of sodalite-haüyne are only found

38 at Kirchberg, whereas the pervasive alteration at Fohberg and Endhalden transformed

39 feldspathoid minerals completely to zeolites.

40 Zeolites formed in a continuously cooling hydrothermal regime after emplacement and

41 solidification of phonolitic magmas. The common paragenetic sequence corresponds to a

42 decrease in the Ca/Na ratio, as well as an increase in the Si/Al ratio with time. The shift

43 from Ca-Na- to pure Na-zeolites is an expression of closed-system behavior in a water-rich

44 environment at Fohberg and Endhalden, which both intruded an Oligocene pre-volcanic

45 sedimentary unit. The late crystallization of K-bearing chabazite-Ca points to a

46 progressively more open hydrothermal system in the Kirchberg phonolite, which was

47 emplaced in a subaerial volcanic succession and was influenced by K-enriched fluid from

2

Revision 1

48   leucite-bearing country rock. Therefore, the geological setting and nature of emplacement

49   are important factors that control the degree of zeolitization of intrusive feldspathoid

50   minerals -bearing rocks and whether a zeolite occurrence can be used as mineral deposit.

51

52   **Keywords**

53   Natrolite, gonnardite, analcime, zeolite, alkaline rocks, phonolite, Kaiserstuhl

Revision 1

INTRODUCTION

54

55

56   Rock alteration and the formation of secondary mineral assemblages are important

57 processes in the genesis of many types of mineral and ore deposits. In fact, most natural zeolite

58 deposits are the result of decomposition of various primary phases in the presence of aqueous

59 fluids. Differences between zeolite deposits exist regarding modal abundances and the

60 mineralogical complexity of the alteration assemblage, from near-monominerallic to highly

61 diverse, which reflects inherent differences in the reacting source rocks, in fluid accessibility and

62 composition, in thermal regime, and in geologic setting (e.g. de'Gennaro and Langella 1996;

63 Ibrahim and Hall 1996; Langella et al. 2013; Weisenberger et al. 2014; Cappelletti et al. 2015;

64 Atanasova et al. 2017).

65   Natural zeolites form a large group of tectosilicate minerals characterized by the common

66 feature of an open framework structure enclosing interconnected pores and channels. The three-

67 dimensional framework is built of SiO_4^{4-} and AlO_4^{5-} tetrahedrons in varying proportions but

68 maximum AlO_4^{5-} is limited to unity with SiO_4^{4-} according to Loewenstein's rule (Loewenstein

69 1954). As a consequence, the aluminosilicate framework contains excess electrons and the walls

70 of zeolitic pores and channels are negatively charged, which allows positively charged ions or

71 bipolar molecules to be fixed in this pore space. Due to the weak bonding strength, these ions and

72 molecules are easily exchanged and replaced by others. The most common extra-framework

73 species in natural zeolites are Na^+, K^+, Ca^{2+} and H_2O, but several other species, mainly alkali and

74 alkali earth metals and NH^{4+}, are also known to be incorporated. Over 80 naturally occurring

75 zeolite species are defined by Coombs et al. (1997), and over 170 known framework types of

76 natural and synthetic zeolites are illustrated by Baerlocher et al. (2007).

4

Revision 1

77   Due to their structure-related physicochemical properties, natural zeolites are an important

78   group of industrial minerals. Technical applications are generally related to their ion-exchange

79   capacity, their reversible dehydration, their regular pore spacing, and their pozzolanic activity,

80   which leads to various applications, e.g water and wastewater treatment (Kalló 2001; Al Dwairi

81   et al. 2014; Ibrahim et al. 2016), heavy metal fixation (Napia et al. 2012), soil remediation

82   (Leggo and Ledésert 2001; Leggo et al. 2010), animal feed (Mercurio et al. 2016), agriculture

83   (Faccini et al. 2015), oeonology (Mercurio et al. 2010), the delivery of certain pharmaceuticals

84   (NSAIDs) by surface modified natural zeoites (e,g. Mercurio et al. 2018), the use of zeolite-rich

85   rocks in ancient roman structures (e.g, Jackson et al. 2017; Izzo et al. 2018), and many more.

86   A major application of natural zeolites is their use in the cement industry as pozzolanic

87   substitute for ordinary portland cement (OPC) (Mertens et al. 2009; Snellings et al. 2010a, 2012;

88   Özen et al. 2016). Natural pozzolans are silicates or alumina-silicates, e.g. zeolites, which are

89   able to react in an alkaline environment with Ca^{2+} commonly found in cement paste or $Ca(OH)_2$

90   in hydrous solution. The reaction products, intergrown hydrated calcium silicates and hydrated

91   calcium aluminates, are comparable to those formed from the hydration of pure OPC (Özen et al.

92   2016). The pozzolanic reaction is a surface-controlled process based on the hydrolysis of Si-O-Si

93   and Al-O-Si bonds (Snellings et al. 2012). Despite the crystallographic characteristics of the

94   zeolite, a large and not fully recognized number of physicochemical parameters affect their

95   reactivity, including extra-framework cation composition and specific surface of the zeolite

96   material (Mertens et al. 2009; Snellings et al. 2010b), and physicoschemical properties of the

97   solution (Snellings et al. 2012). Although not studied systematically yet on pure zeolite phases

98   with controlled conditions, it becomes evident that the pozzolanic reactivity is a general feature

99   of natural zeolites (Mertens et al. 2009; Özen et al. 2016).

5

Revision 1

100   Economic deposits of natural zeolites are commonly related to vitreous tuffs from which

101   they formed by decomposition and hydration of volcanic glass. Deposits of this kind are found

102   worldwide in regions of young explosive volcanism (e.g. Cochemé et al. 1996; de'Gennaro and

103   Langella 1996; Ibrahim and Hall 1996; Cappelletti et al. 2015; Özen et al. 2016), Furthermore,

104   there are also examples of zeolite occurrences in intrusive alkaline rocks (Tschernich 1992 and

105   references therein; Schilling et al. 2011; Weisenberger et al. 2014) and their metamorphosed

106   counterparts (Tschernich 1992 and references therein; Chakrabarty et al. 2016; Atanasova et al.

107   2017).

108   In the alkaline rock-carbonatite complex of the Kaiserstuhl in southwest Germany, several

109   phonolite intrusions occur which show variable degrees of zeolitization. Despite general

110   similarities in their primary magmatic composition, they exhibit differences in zeolite-dominated

111   alteration, both in quantity (i.e., in their grade) and in mineralogical characteristics, which leads

112   either to economic zeolite deposits, or to non-economic zeolite occurrences. By studying the

113   mineralogy and the compositional variations of zeolites in the Kaiserstuhl phonolites, and

114   relating the observations to the geologic setting of each occurrence, we define factors necessary

115   for the formation of economic zeolite deposits in the alkaline intrusive rocks of the Kaiserstuhl

116   Volcanic Complex, which can be adopted for similar occurrences elsewhere.

117

118   **THE KAISERSTUHL VOLCANIC COMPLEX**

119

120   The Miocene Kaiserstuhl Volcanic Complex (KVC) is located in the southern part of the

121   Upper Rhine Graben, SW Germany (Fig. 1), close to the city of Freiburg. The KVC belongs to

122   the Central European Volcanic Province (Wimmenauer 1974) characterized by generally SiO_2-

123   deficient, alkaline intraplate volcanism, formed in the course of the Alpine continent-continent

124   collision (Wedepohl et al. 1994; Wilson and Downes 1991). The KVC is the only larger

125   polygenetic volcanic edifice in the Upper Rhine Graben, but highly silica-undersaturated alkaline

126   dikes and diatremes are common in the graben and along its shoulders. These are represented by

127   the Black Forest, Vosges and Odins Forest crystalline complexes, and also in their overlying

128   Mesozoic to early Cenozoic sedimentary cover, which is locally preserved inside the graben and

129   along its margins. They are classified as olivine-melilitites and olivine-nephelinites and are

130   considered unfractionated products of low percentage partial mantle melts (Keller 2001), carrying

131   lherzolitic xenoliths (Keller et al. 1997).

132   The Kaiserstuhl can be subdivided into two different major geologic units (Figure 1). (1)

133   The eastern part consists of a sequence of Paleogene sediments (marls, sandstones and

134   limestones) in a north-south oriented prevolcanic horst structure. (2) The central-western part

135   consists of volcanic rocks, whereas the central part is formed by a subvolcanic intrusive complex

136   surrounded by effusive and explosive volcanics in the north, west and south. The Kaiserstuhl

137   most likely had the structure of a complex stratovolcano, or a volcanic field with eruptions from

138   various volcanic centers (Keller 2001).

139   Petrologically the rocks of the KVC form a series from primitive olivine nephelinites

140   towards slightly fractionated basanites, tephrites and finally phonolites, which were derived from

141   two different parental magmas (Braunger et al. 2018). Carbonatites and carbonate-melilite-

142   bearing silicate rocks ('bergalite') occur in close relationship to nephelinitic diatreme brecciae in

143   the subvolcanic center of the volcanic complex (Keller 2001).

144   Activity emerged with the eruption of olivine-nephelinites (19.0 ± 1.6 Ma, whole-rock K-

145   Ar age; Baranyi et al. 1976), the deposition of mainly tephritic pyroclastites and lavas (18.2 –

146   16.5 Ma) and the emplacement of various subvolcanic intrusions and dikes between 18.4 and

147   15.3 Ma (Wimmenauer 2003 and references therein). Volcanism ceased with the eruption of the

7

Revision 1

148   parasitic Limberg-Lützelberg complex at the northwestern margin of the KVC, where a

149   phonolitic tuff was deposited at 16.2 ± 0.2 Ma (Kraml et al. 2006) in a nephelinite-basanite-

150   tephrite-phonolite sequence.

151

152   **Phonolites in the KVC**

153

154   Phonolites form one of the major petrologic families in the KVC and are subordinate in

155   volume only to the rocks of the tephritic family, from which they are derived by fractionation

156   (Braunger et al. 2018). They occur as intrusive subvolcanic stocks and dikes, and as pyroclastic

157   products of explosive volcanic activity. Members of the phonolitic family are recognized by the

158   modal mineralogy: sodic pyroxene (aegirine-augite), alkali feldspar, titanian andradite

159   ('melanite') and sodalite/haüyne. Phonolites from the eastern KVC (Fig. 1) form a distinct

160   subgroup characterized by the presence of wollastonite. These intrusions are apparently arranged

161   on a straight N-S striking line which parallels a major fault located about 1-1.5 km to the west.

162   Larger occurrences of phonolite are found in three different geologic settings in the Kaiserstuhl

163   volcanic edifice (Fig. 1): (1) as intrusions in the subvolcanic center, in close spatial relationship

164   to essexitic and carbonatitic intrusions; (2) as intrusions emplaced into the prevolcanic Oligocene

165   sediments of the eastern Kaiserstuhl (Fohberg, Endhalden); (3) as intrusion in subaerial, mainly

166   tephritic pyroclastites and lavas in the western KVC (Kirchberg).

167   Varieties of phonolite *sensu lato* occur as small-volume bodies in the KVC. They are

168   represented by dm- to m-thick dikes of tinguaite (feldspar-foid ratio 1:1 – 1:10), and

169   haüynophyre (Wimmenauer 1962) and leucitophyre (Keller 1964; Spürgin et al. 2008), both with

170   a feldspar-foid ratio of <1:10.

8

Revision 1

171   The plutonic facies of the phonolitic family is represented by sodalite syenites (locally

172   more mafic 'ledmorite'), and foidolites ('tawite'). They are mineralogically related to phonolites,

173   but with a distinct coarse-grained texture. Occurrences are limited to xenoliths, especially in the

174   Kirchberg phonolite (Czygan 1977), and to the subvolcanic center of the KVC, where ledmorite

175   is recorded as major rock type in a drill core (Wimmenauer 1962, 2003).

176

177   **Zeolites in the KVC**

178

179   All silicic lithologies of the KVC were affected by subsequent alteration and zeolitization

180   to variable degrees. Zeolites occur as vesicle-fillings, in fracture assemblages or as fine-grained

181   groundmass replacing components. Processes responsible for alteration include hydrothermal

182   decomposition of primary igneous phases, particularly minerals of the feldspathoid group

183   (Weisenberger et al. 2014), and decay and hydration of volcanic glass either in a hydrothermal or

184   a hydrous low-temperature environment (Eggleton and Keller 1982; Weisenberger and Spürgin

185   2009). The following zeolite species are reported from the KVC by Weisenberger and Spürgin

186   (2009), Weisenberger et al. (2014) and Marzi and Spürgin (2017): Analcime, chabazite-Ca,

187   faujasite-Na, faujasite-Mg, gonnardite, merlinoite, mesolite, natrolite, offretite, phillipsite-K,

188   phillipsite-Ca, and thomsonite-Ca.

189

190   **ANALYTICAL METHODS**

191

192   Mineral compositions were determined by electron probe microanalysis (EPMA) at the

193   University of Oulu using a JEOL JXA-8200 electron microprobe. Operating conditions were 15

194   kV acceleration voltage and 15 nA beam current with counting times of 10 s. Zeolites were

9

Revision 1

195   analyzed with a defocused beam (20 μm). Sodalite-haüyne was analyzed with a beam diameter of

196   5 or 10 μm. Na and K were measured first, to minimize the effect of Na and K loss during

197   determination. Since zeolites lose water when heated, the rock samples and crystals were

198   mounted in epoxy resin to minimize loss of water. Natural and synthetic standards were used for

199   calibration. The charge balance of zeolite formulas is a reliable measure for the quality of the

200   analysis. It correlates with the extent of thermal decomposition of zeolites during microprobe

201   analysis. A useful test is based on the charge balance between the non-framework cations and the

202   amount of tetrahedral Al (Passaglia 1970). Analyses are considered acceptable if the sum E% =

203    $100 \times [Al-(Na+K)-2(Ca+Sr+Ba)]/[(Na+K)+2(Ca+Sr+Ba)]$ of the charge of the extra-framework

204   cations (Ca^{2+}, Sr^{2+}, Ba^{2+}, Na^+, and K^+) is within 7% of the framework charge.

205   Mineralogical compositions were determined on bulk-rock samples of each phonolite by

206   powder X-ray diffractometry (PXRD) using a Bruker D2 Phaser diffractometer. For this purpose,

207   rock samples of 2-4 kg were crushed, homogenized and representative subsamples of 50 g were

208   finely ground in a laboratory mill. Scans with Cu Kα radiation were recorded in the range $5° < 2θ$

209    $< 70°$ with a step width of 0.016° and an integration time of 2s/step. Full-pattern Rietveld based

210   quantitative phase analyses (QPA) were performed with the Bruker TOPAS software applying a

211   fundamental parameters procedure (Cheary and Coelho 1992; Madsen and Scarlett 2008).

212   Instrumental contributions to the recorded patterns were initially refined on a sample of LaB_6. In

213   the first step of QPA of the phonolite samples, the unit cell parameters of each phase have been

214   refined to match the observed peak positions. In a second step, the crystallite size and strain

215   functions have been applied to model the peak shape. Further, atomic positions have been

216   allowed to refine in narrow limits, and in order to limit the number of independently refined

217   parameters, an overall isotropic thermal factor B_{eq} was refined for all atomic sites in all phases.

10

Revision 1

218   Due to the holocrystalline nature of the phonolites, no amorphous phase content has been refined.

219   Results of QPA are listed in Table 2.

220   Thermogravimetry (TG) and differential thermal analysis (DTA) were performed at the

221   Institute for Technology of Nuclear and Other Mineral Raw Materials (ITNMS). Thermal

222   analysis was performed on a Netzsch STA 409 EP (Selb, Germany). Samples were put in ceramic

223   crucibles and heated (20 – 1000ºC) in an air atmosphere with a heating rate of 10ºC/min^{-1}.

224   Mineral stabilities were obtained using the program SUPCRT92 (Johnson et al. 1992),

225   employing the slop98 database and thermodynamic data from Helgeson et al. (1978) and Neuhoff

226   (2000). Reactions were calculated considering low quartz activity and aluminum conservation in

227   the solid phases.

228

229   **RESULTS**

230

231   **Mineralogy and Petrology of Phonolite Localities**

232

233   The three largest phonolite stocks of the KVC, two of them located in the eastern (Fohberg,

234   Endhalden) and one in the western (Kirchberg) Kaiserstuhl (Fig. 1), have been investigated

235   during this study. Their petrographic characteristics are summarized in Table 1. Other known

236   occurrences of intrusive phonolites in the subvolcanic center of the KVC, as well as phonolitic

237   dikes and pyroclastites (Wimmenauer 1962, 2003) have not been considered due to their high

238   degree of weathering in surficial outcrops and their low economic potential regarding minerals of

239   the zeolite group.

240

11

Revision 1

241   **Fohberg Phonolite.** The Fohberg phonolite, 600 x 450 m in aerial size, is the largest

242   phonolite body in the eastern Kaiserstuhl and probably, as outcrop conditions of phonolites in the

243   central KVC allow no correlation and reconstruction, also the largest one in the entire KVC. It

244   intruded a series of Oligocene sediments of the Pechelbronn Formation, mainly marl, limestone

245   and calcareous sandstone (Wimmenauer 2003), and is cut by a dike of porphyritic essexite.

246   The petrography of the Fohberg phonolite was investigated by Wimmenauer (1962), and

247   data on the primary and secondary mineralogy is found in Weisenberger et al. (2014). The rock

248   has a slightly porphyritic texture with phenocrysts (≤ 3 mm) of feldspathoid minerals, aegirine-

249   augite, wollastonite and andradite in a greenish-grey fine- to medium-grained matrix of sanidine,

250   aegirine-augite and feldspathoid minerals (Fig. 2a,b). Phenocrysts are in general euhedral;

251   however, garnet phenocrysts tend to be subhedral due to possible corrosion. Late magmatic

252   decomposition of mafic phases formed accessory titanite and götzenite, a F- and LREE-bearing

253   Ca-Ti silicate of the rosenbuschite group (Czygan 1973; Albrecht 1981; Weisenberger et al.

254   2014).

255   A prominent feature of Fohberg phonolite samples is the complete decomposition of

256   feldspathoid minerals, and the partial replacement of wollastonite. Secondary minerals, which

257   also form large portions of the matrix, include natrolite as sole Na-zeolite endmember,

258   gonnardite, minor thomsonite (both Ca-Na zeolite species), and calcite. Additionally, pectolite

259   and sepiolite occur in minor quantities as alteration products (Weisenberger et al. 2014).

260   On an outcrop scale, and in contrast to the Endhalden and Kirchberg phonolites, the

261   Fohberg phonolite hosts a network of numerous, mainly steep dipping fractures. These are

262   partially or totally filled with a secondary zeolite-dominated assemblage similar to the altered

263   rock matrix. A temporal succession from Ca-Na species (thomsonite, gonnardite) to pure Na-

12

Revision 1

264   zeolite (natrolite) is observed (Weisenberger et al. 2014), followed by later phases, e.g.

265   apophyllite, fluorite and calcite (for a full list see Marzi 1983).

266   The phonolite at Fohberg is mined by Hans G. Hauri KG Mineralstoffwerke, Bötzingen.

267   Several applications of the rock powder are directly related to its zeolite content and include the

268   use as pozzolan in the cement and concrete industry (Kassautzki 1983), and as cattle feed

269   additive.

270

271

272   **Endhalden Phonolite.** The Endhalden phonolite covers an area of approximately 450 x

273   250 m and is located about 1 km to the north of the Fohberg phonolite (Fig. 1). It is also in

274   contact to sediments of the Pechelbronn Formation (Wimmenauer 2003), but no physical

275   connection between the Endhalden and the Fohberg phonolite bodies is exposed or known, which

276   can indicate their co-genetic formation.

277   The shape and structural position of the Endhalden phonolite is not clarified yet. Shallow

278   vertical drill cores indicate that the Endhalden phonolite is emplaced on top of a clay-dominated

279   sedimentary unit. It may represent a shallow intrusive body like a sill, small laccolith, or

280   cryptodome, or a subaerial feature like an erosional remnant of a thick lava flow or extrusive

281   dome.

282   Petrographically the Endhalden phonolite closely resembles the Fohberg phonolite. It is

283   weakly porphyritic to various degrees, with a similar set of phenocrysts (feldspathoid minerals,

284   sanidine, aegirine-augite, wollastonite, andradite) within a medium- to fine-grained groundmass

285   of sanidine, aegirine-augite and feldspathoid minerals (Fig. 2c,d). K-feldspar and feldspathoid

286   minerals often show a poikilitic texture hosting very-fined-grained aegirine-augite inclusions.

13

Revision 1

287   As in the Fohberg phonolite, all primary igneous feldspathoid minerals are completely

288   replaced by zeolites and calcite. Wollastonite is always decomposed. In contrast to the Fohberg

289   alteration assemblage, analcime occurs as a second Na-endmemeber zeolite together with

290   natrolite, and minor mesolite is found as an additional Ca-Na species besides gonnardite and

291   thomsonite.

292   The Endhalden phonolite is unique as it exhibits only very limited hydrothermal fracturing,

293   but is rich in vesicles, up to 1.5 cm in size, which often contain euhedral zeolite fillings (analcime

294   and/or natrolite), particularly in the upper part of the phonolite body.

295

296   **Kirchberg Phonolite.** With an extent of 430 x 200 m, the Kirchberg phonolite is the only

297   stock-like body intruding pyroclastites and lavas of the subaerial volcanic facies of the western

298   KVC. It is in intrusive contact to tephritic ash tuffs to tuff breccia, and to carbonatitic ash- to

299   lapilli tuffs. Rafts of country rock occur in the outermost 10-20 m of the phonolite stock. Along

300   the contact zone to subaerial country rock, the grey-brown colored phonolite grades into light

301   grey marginal facies.

302   The petrography of the Kirchberg phonolite was reported by Wimmenauer (1962). Despite

303   general similarities, it shows characteristic differences compared to the Fohberg and Endhalden

304   phonolites. The porphyritic texture is less developed, dominated by groundmass phases, resulting

305   in a fine- to medium-grained texture. Apart from the characteristic set of phases for phonolites in

306   the KVC (haüyne, sanidine, aegirine-augite, andradite), the Kirchberg phonolite contains

307   phenocrysts of euhedral to corroded plagioclase, which are often overgrown by K-feldspar. In

308   contrast to the Fohberg and Endhalden phonolites, the Kirchberg phonolite contains no

309   wollastonite, but fresh grains of haüyne and sodalite (Wimmenauer 1962; Spürgin et al. 2014),

310   pigmented by hematite, are common (Fig. 2e).

14

Revision 1

311   Although the Kirchberg phonolite is also affected by zeolite-forming alteration (Fig. 2f),

312   the intensity is very heterogeneous and less pronounced than in the phonolites from the eastern

313   KVC. The secondary assemblage contains natrolite, thomsonite, gonnardite and chabazite-Ca,

314   and minor amounts of clay minerals. Additional secondary minerals, generally found in fractures,

315   are listed by Wimmenauer (1962) and include calcite, apophyllite, gypsum and others.

316

317   **Quantitative mineralogy**

318

319   The results of bulk-rock PXRD and QPA (Table 2) show the mineralogical composition of

320   the three phonolites. The Fohberg and Endhalden phonolites show the highest zeolite contents

321   with proportions X_{Zeo} = Zeo/(Zeo+Fsp) in the range of 0.3-0.6. Gonnardite is the major zeolite

322   species in one sample (Fohberg_7) and accounts to approximately 10-20 percent of the total sodic

323   zeolite content (natrolite, gonnardite, analcime; X_{Gon} = Gon/(Ntr+Gon+Anl) = 0.1-0.2) in the

324   other samples. Analcime is restricted to the Endhalden phonolite, where also the calcite content is

325   notably higher. Low total zeolite contents in combination with the presence of clay minerals in

326   sample Endhalden_5 are an expression of surficial weathering in the outcrop.

327   In contrast, the Kirchberg phonolite contains a higher amount of alkali feldspar and, in one

328   case (Kirchberg_4) also intermediate plagioclase as well as less clinopyroxene and no

329   wollastonite. Zeolite contents are highly variable. The mineralogy of sample Kirchberg_3

330   resembles those from Endhalden except a high gonnardite content which is reflected by X_{Gon} =

331   0.42, but in other samples only minor quantities of zeolites (gonnardite and chabazite) could be

332   identified. Sodalite-haüyne, which is known to occur at Kirchberg, was detected by PXRD in two

333   samples but could not readily be quantified. The content of sodalite-haüyne is believed to be

334   underestimated and should be in the order of more than ten percent, according to thin section

15

Revision 1

335   observations. Wimmenauer (1962) reports an average of 61 vol% feldspar and 28 vol% sodalite-

336   haüyne, including products of its decomposition.

337

338   **Zeolite chemistry and paragenesis**

339

340   Zeolite phases were identified and characterized using PXRD and EPMA, except mesolite

341   which was only detected by EPMA due to its rarity and very small grain size. The chemical

342   composition of zeolite species is presented in Table 3 and Figure 3. Considering the ternary

343   system Ca-Na-K the following succession is observed with decreasing Ca concentrations:

344   thomsonite-gonnardite-natrolite-analcime. Textural relationships in alteration assemblages

345   indicate that this chemical trend defines a common temporal succession. In addition, chabazite is

346   observed only in the Kirchberg phonolite, where it occurs as the latest generated zeolite.

347   **Gonnardite.** Gonnardite is generally less abundant than natrolite, but may reach similar

348   concentrations in some parts of the Fohberg phonolite. It is an early crystallizing secondary phase

349   of the rock matrix, and forms an early phase of fissure assemblages, where it nucleates at the

350   fissure walls and is overgrown by natrolite. Gonnardite compositions from Fohberg

351   (Weisenberger et al. 2014) and Endhalden form a continuous trend from Na-Al- ($T_{Si} = 0.55$)

352   towards Ca-Si-rich compositions ($T_{Si} = 0.59$), whereas Kirchberg gonnadite is chemically distinct

353   due to considerably higher Na concentrations at moderate T_{Si} (0.56). Gonnardite analyses from

354   the Fohberg and Endhalden localities yield Sr concentrations up to 0.39 atoms per formula unit

355   (apfu). It cannot be excluded that this elevated Sr concentration may result from submicroscopic

356   inclusions of another Sr-bearing phase (e.g. thomsonite).

357   **Thomsonite-Ca.** Thomsonite-Ca is occasionally present as early-formed secondary phase

358   in all three phonolites (Fig. 2f). It has the lowest Si/Al ratio ($T_{Si} = 0.52$) of all zeolites found in

16

Revision 1

359   the KVC (Weisenberger and Spürgin 2009), and at Fohberg and Endhalden, it is the most Ca-rich

360   zeolite species. Thomsonite-Ca from Endhalden is Sr-rich with a maximum content of 3.16 Sr

361   apfu (equal to 26 percent of extra-framework cations).

362   **Mesolite.** Mesolite is an infrequent Ca-Na-zeolite in the Fohberg and Endhalden

363   phonolites. Chemical analyses of the Endhalden mesolite are close to the ideal stochiometric

364   composition ($T_{Si} = 0.59$). Weisenberger et al. (2014) report thin, elongate mesolite inclusions of

365   approximately 1 x 50 μm with a growth orientation along the c-axis in large natrolite grains from

366   the Fohberg phonolite.

367   **Natrolite.** Natrolite is present in all KVC phonolites, and it is the dominant zeolite species

368   in the Fohberg and the Endhalden phonolites. It forms cm-large, transparent euhedral needles in

369   fissures of Fohberg and Kirchberg, and smaller crystals in vugs of Endhalden. Furthermore,

370   natrolite is a major phase in the Fohberg groundmass, and to a lesser degree in the Endhalden

371   phonolite. It is preceded by gonnardite and thomsonite-Ca, and overgrown by analcime, calcite

372   and other minerals of the secondary assemblage (Marzi 1983), where present. Especially at the

373   Endhalden locality, natrolite may contain distinct amounts of Ca (up to 0.47 apfu) based on 80

374   framework oxygens), which is also a common feature seen in analyses from other occurrences

375   (Ibrahim 2004; Çiftçi et al. 2008; Kónya and Szakáll 2011). Concentrations of all other

376   exchangeable cations are negligible, and T_{Si} shows only limited variations with an average value

377   of 0.61

378   **Analcime.** Besides natrolite, analcime is the characteristic zeolite species in the Endhalden

379   phonolite. It is part of the rock matrix and also forms clear, euhedral crystals several mm in size

380   filling open vugs. Petrographic observations indicate that analcime always postdates natrolite,

381   and it may be overgrown by anhedral masses of calcite. Most analcime analyses show near-

17

Revision 1

382   endmember composition, in a few cases with minor incorporation of K-component. It is the most

383   Si-rich ($T_{Si} = 0.67$) zeolite species in the Endhalden phonolite.

384   **Chabazite-Ca**. Chabazite-Ca is sporadically found in the groundmass of the Kirchberg

385   phonolite (Table 2 and Fig. 2f). It shows a wide compositional range in Si-R^{2+}-R^+ space and is

386   the only zeolite species in KVC phonolites which incorporates a significant K component. It has

387   a highly variable Si/Al-ratio ($0.56 < T_{Si} < 0.72$) and is the most Si-rich zeolite at Kirchberg (Fig.

388   3).

389   **Other secondary minerals.** Calcite is found in variable proportions as a secondary

390   alteration product in all phonolites. In contrast to the Fohberg and Kirchberg phonolites, where

391   calcite appears as minor alteration phase, the Endhalden phonolite exhibits larger quantities of

392   calcite (Table 2). Chemical analyses reported by Weisenberger et al. (2014) from Fohberg

393   indicate pure calcium carbonate with only very little incorporation of Mn (0.02 apfu) and Fe

394   (0.01 apfu)

395   Minor quantities of clay minerals are found within the phonolite intrusions. During electron

396   probe microanalysis a platy mineral phase has been observed filling interstitial pores in the

397   Kirchberg phonolite. Silica and Al are the dominant cations with a Si/Al ratio of about 1 and

398   variable trace amounts of Fe, Mg and Ca. A subsequent X-ray diffraction analysis of the sample

399   indicated that the most likely phase is halloysite ($Al_2Si_2O_5(OH)_4$). Sepiolite and pectolite have

400   been described by Weisenberger et al. (2014) in the Fohberg phonolite as minor alteration

401   products.

402   Various other secondary minerals, which generally postdate the zeolite assemblages of

403   fissures in the Fohberg and Kirchberg phonolites, are reported by Wimmenauer (1962) and Marzi

404   (1983).

405

18

Revision 1

406   **Thermal behavior**

407

408   The thermal behavior of bulk-rock samples was determined by TG-DTA, the results are

409   shown in Figure 4. Samples from Endhalden and Fohberg show pronounced weight loss steps in

410   the temperature intervals of 300-380°C and ca. 700-800°C, which correspond to the single-step

411   dehydration of natrolite and the calcination of calcite, respectively (van Reeuwijk 1972; Deer et

412   al. 2004; Rodriguez-Navarro et al. 2009). Although natrolite is the thermally most active

413   mineralogical phase, contributions of other phases, like other minor zeolite species and clay

414   minerals, cannot be excluded. The reactions of natrolite and calcite are reflected by strong

415   endothermal peaks in DTA plots (Fig. 4). Furthermore, a steady weight loss in the region below

416   300°C, and additional minor endothermal signals slightly below 100°C, at 200-250°C and at 460-

417   480°C, is evident in sample Fohberg_7. These are related to the multistep dehydration and final

418   structure collapse of abundant gonnardite in this sample (van Reeuwijk 1972). The effect of

419   analcime dehydration, which contributes to a general weight loss in the region from 250°C to

420   450°C (Harada and Nagashima 1972), remains largely unresolved in the Endhalden samples. It is

421   only evident by a very minute endothermal signal at 300°C, on the low-temperature flank of the

422   large natrolite peak.

423   The Kirchberg phonolite shows the largest variations with individual patterns for each

424   sample. Sample Kirchberg_3 is dominated by natrolite dehydration and shows no further

425   reactions except a steady weight loss below 300°C, whereas the reaction curves of samples

426   Kirchberg_4 and Kirchberg_5 are combined patterns of zeolite dehydration, clay dehydration and

427   calcination of calcite in variable proportions.

428

429   **DISCUSSION**

          19

Revision 1

430

431 **Zeolite precursor phase**

432

433   All phonolites investigated in this study are holocrystalline subvolcanic intrusive rocks. No

434 evidence is found for the presence, or the former presence, of volcanic glass, which is an

435 important zeolite precursor phase in many zeolite deposits elsewhere formed from vitreous

436 volcanic tuffs. However, the presence of feldspathoid minerals as members of the pyrogenic

437 assemblages is evident in all three phonolites. They occur as dominant phenocryst phases,

438 ranging in diameter between 0.1 and 1 mm (Fig. 2a,e), and as a fine-grained matrix phase.

439 Pseudomorphic aggregates of replaced feldspathoids in all three phonolites commonly show a

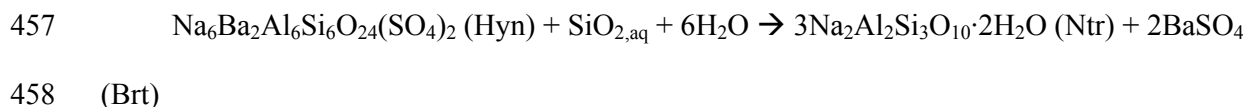440 dark or orange rim, which may be caused by submicroscopic inclusion of Fe-phases.

441   Unaltered phenocrysts of feldspathoids are only found in the Kirchberg phonolite. The

442 chemical composition is shown in Table 4 and Figure 5. Sodalite-group mineral classification

443 based on the Ca-Na-K system indicates that this feldspathoid mineral is haüyne. Classification by

444 volatiles implies that the SO_3 concentrations are underestimated by electron probe microanalysis,

445 which may also explain the low totals (Table 4). However, the Kirchberg phonolite shows a

446 heterogeneous alteration and haüyne may be replaced by secondary minerals like zeolites

447 (chabazite, gonnardite, natrolite, and thomsonite) and calcite.

448   Phenocrysts and matrix feldspathoid minerals in the Fohberg and Endhalden phonolites are

449 totally altered to aggregates of fibrous spherulitic zeolites (including analcime, natrolite,

450 thomsonite, and gonnardite), calcite and barite, leaving pseudomorphs with characteristic

451 hexagonal and rhombic dodecahedral shape and few rectangular cross-sections (Fig. 2a). The

452 common association of barite grains with these pseudomorphic aggregates (Fig. 2b), in

453 combination with the geometry of the aggregates, points to an S/SO_4-bearing sodalite group

20

Revision 1

454 mineral as precursor phase, e.g. haüyne or nosean. The following reaction shows the breakdown

455 of a hypothetical barium component in haüyne to natrolite and barite:

456

457 $Na_6Ba_2Al_6Si_6O_{24}(SO_4)_2$ (Hyn) + $SiO_{2,aq}$ + $6H_2O$ → $3Na_2Al_2Si_3O_{10} \cdot 2H_2O$ (Ntr) + $2BaSO_4$

458 (Brt)

459

460   However, no unaltered relics of feldspathoid minerals have been identified in the Fohberg

461 (Weisenberger et al. 2014) and Endhalden phonolites so far. Highly Ba-enriched beforsite (Keller

462 2001), which is found as late-stage centimeter-sized veins within the carbonatite complex of the

463 central KVC (Fig. 1), may also account as a source of Ba. However, it occurs in a spatially and

464 geologically different context and is volumetrically insignificant, therefore it is assumed that Ba

465 is locally derived and precipitated as barite in the phonolite alteration assemblages.

466

467 **Hydrothermal alteration**

468

469   **Degree of alteration.** As described by Weisenberger et al. (2014) for the Fohberg

470 phonolite, the conversion of an essentially anhydrous primary mineralogy to a zeolite-dominated

471 and therefore water-rich assemblage and the syn- to post-deformation mineralization and healing

472 of brittle fractures is likely a scenario of hydrothermal overprinting of the Fohberg phonolite

473 body during post-magmatic cooling and late stage circulation of meteoric fluids. Although

474 fracturing and fracture mineralization within the Endhalden and Kichberg phonolites are limited,

475 a similar scenario of sub-solidus alteration during post-magmatic cooling and late stage

476 circulation of meteoric fluids is applicable.

21

Revision 1

477   In general, the secondary mineralogy is very similar in all three phonolites, showing the

478   same general trend from early formed Ca-Na zeolites towards Na-dominated zeolites during

479   subsequent alteration. Nevertheless, alteration shows differences that are rather controlled by

480   fluid-rock interaction and the physicochemical properties of the fluid than by the primary

481   chemical and mineralogical composition of the host rock.

482   Sub-solidus alteration is marked by the breakdown of haüyne as the dominant feldspathoid

483   mineral. In addition, partial wollastonite breakdown occurs in the Fohberg (Weisenberger et al.

484   2014) and Endhalden phonolites, as wollastonite is only present there. Plagioclase, which only

485   occurs in the Kirchberg phonolite, shows no sign of alteration and gives evidence for the limited

486   overall alteration of the Kirchberg phonolite. The hydrothermal alteration within the two eastern

487   phonolites (Fohberg and Endhalden) is pervasive, secondary minerals replace all primary

488   feldspathoid minerals. The intensity of wollastonite breakdown in the Fohberg phonolite is very

489   heterogeneous from fresh grains towards fully decomposed ones, in contrast to the Endhalden

490   phonolite where wollastonite is completely replaced. The degree of alteration within the

491   Kirchberg phonolite differs significantly as it still contains primary haüyne, with only limited

492   zeolite- and clay-forming alteration. The change in degree of alteration between the Kirchberg

493   phonolite and the two phonolites within the eastern part of the KVC is directly related to

494   differences in the country rocks in which the phonolites have been intruded (Fig. 6). The

495   Kirchberg phonolite is emplaced into a pile of volcanic rocks, whereas the two eastern phonolites

496   are situated within a prevolcanic sedimentary sequence of lime- and mudstones (Wimmenauer

497   2003). A stable isotope study of secondary calcite from the Fohberg phonolite (Weisenberger et

498   al. 2014) suggests that fluids were derived from the surrounding sedimentary succession. In

499   contrast, $^{87}Sr/^{86}Sr$-isotope studies (Wimmenauer 2010; Weisenberger et al. 2014) suggest that Ca,

500   as major constituent in secondary minerals of the phonolites, is locally derived from the

22

Revision 1

501   magmatic parent rock. This indicates that the lime- and mudstones have been dehydrated during

502   the emplacement of the phonolites, and aquifers in these lithologies have been tapped and drained

503   into the cooling phonolite intrusions. This is supported by the contact metamorphic overprint of

504   the underling mudstone of the Endhalden phonolite, in which a dehydration front is developed

505   (Spürgin et al. 2014). The Kirchberg phonolite, in contrast, intruded a sequence of subaerial lavas

506   and pyroclastites. Although the volcanic pile shows evidence of alteration due to the

507   emplacement of the Kirchberg phonolite, the thermal alteration of nearly anhydrous volcanic

508   rocks does not have the potential to deliver volatiles that could cause a pervasive alteration of the

509   Kirchberg phonolite.

510   It is noted by previous studies on phonolite tuff deposits that fluid accessibility controls the

511   alteration of volcanic products and the formation of zeolites (e.g. de´Gennaro et al. 2000;

512   Bernhard and Barth-Wirsching 2002). However, within some pyroclastic deposits the formation

513   of zeolites is related to groundwater flow (de´Gennaro et al. 2000; Hay and Sheppard 2001;

514   Bernhard and Barth-Wirsching 2002). In contrast, the alteration within intrusions is more related

515   to the presence and the accessibility of fluids, and open system behavior during sub-solidus

516   cooling and deviation from auto-metasomatic conditions. Thereby, for the two eastern phonolites

517   the thermal regimes are assumed to represent near auto-metasomatic conditions, with externally

518   derived fluids from the surrounding sediments infiltrating into the sub-solidus cooling intrusions,

519   as it was postulated for the Fohberg phonolite by Weisenberger et al. (2014). In contrast, the

520   Kirchberg phonolite indicates open system behavior, as a result of a thermal and maybe a

521   chemical gradient within the hydrothermal system. The open system behavior of the Kirchberg

522   phonolite is further supported by the very limited amount of natrolite, indicating only a limited

523   fluid change during hydrothermal evolution, most likely caused due to local disequilibrium, even

524   though a Na depletion is observed within the Ca-Na zeolites. Furthermore, all analyzed samples

23

Revision 1

525   from the Kirchberg phonolite yield different alteration assemblages. During experimental studies

526   Barth-Wirsching and Höller (1989) noted that the effect of solution chemistry and reaction time

527   is greater in open systems, whereas the influence of the starting material may entirely be

528   eliminated by material transport possible in an open system. This can explain the variability in

529   alteration of the Kirchberg samples. In contrast, the two eastern phonolite intrusions exhibit large

530   quantities of both Ca-Na and Na zeolites in a temporal succession; these species are present

531   throughout all samples with only minor variations, indicating a closed system behavior (Hay and

532   Sheppard 2001).

533

534   **Fluid evolution.** Fluid evolution can be illustrated in the systems Al_2O_3–SiO_2–CaO–Na_2O–

535   H_2O (Fig. 7) and Al_2O_3–SiO_2–Na_2O–H_2O (Fig. 8) and in terms of mineral stability as function of

536   aqueous species (Ca^{2+}, Na^+, $SiO_{2,aq}$, H_2O) at low temperature and pressure.

537   Figure 7 illustrates the change in fluid composition during the hydrothermal replacement as

538   a function of aqueous cation (Ca^{2+}, Na^+) to hydrogen ion activity ratios at temperatures of 50 and

539   100°C, and pressure of 10 MPa. The overall topology of stability fields does not change with

540   small variations of pressure; therefore, the uncertainty of the emplacement depth can be ignored.

541   Due to a lack of reliable thermodynamic data for gonnardite, mesolite appears instead as

542   intermediate Ca-Na zeolite (Rogers et al. 2006). The chemical evolution of fluids during zeolite

543   formation can be expressed by the observed sequence marked by Ca-Na zeolite species and

544   natrolite (Fig. 7). At higher SiO_2 activity analcime appears instead of natrolite.

545   Similar sequences are observed in basaltic lavas in the Disko–Nuussuaq region, West

546   Greenland (Neuhoff et al. 2006; Rogers et al. 2006) and in the Kahrizak area, Iran (Kousehlar et

547   al. 2012), and are interpreted to have formed in a chemically distinct alteration style that reflects

548   the less Ca and Si-rich primary compositions of these lavas in contrast to provinces with more

24

Revision 1

549   evolved basaltic rocks, like in Iceland (Neuhoff et al. 1999; Weisenberger and Selbekk 2009) or

550   East Greenland (Neuhoff et al. 2006).

551   The alteration mineralogy within the three phonolite bodies shows a general compositional

552   shift from clay minerals (halloysite) to Ca-Na zeolite species (gonnardite, thomsonite, mesolite)

553   and further to the Na endmembers natrolite and analcime. Ca-Na zeolites, in particular

554   thomsonite and gonnardite can locally incorporate higher Sr concentrations (Table 2). However,

555   no systematic Sr distribution is observed and the incorporation of Sr may be caused by local Sr

556   inhomogeneities either within the primary phases or within fluids. The paragenetic sequence

557   corresponds to a decrease in the Ca/Na ratio, as well as an increase in the Si/Al ratio with time

558   (Fig. 3). Nevertheless, a single phonolite body does not cover the entire mineral sequence. The

559   general sequence is characterized by the appearance of thomsonite and gonnardite and followed

560   by natrolite. Fluid-rock interaction results into the evolution of Ca-Na zeolites with a general

561   shift to Na-dominated zeolites. However, textural relations (Fig. 2) suggest that the sequence is

562   developed in an open system environment where the chemical gradient is developed by a change

563   in the fluid fronts.

564   The Kirchberg sequence is characterized by the stability of clay and chabazite. The crystal

565   chemistry of chabazite (Fig. 3) is unique as it is the only zeolite species found in this study that is

566   able to accommodate a significant amount of potassium. The occurrence of late potassium

567   bearing chabazite, which postdates the Ca-Na zeolite succession, suggests the infiltration of

568   meteoric water with high calcium and potassium concentration whose composition became a

569   significant component in total fluid composition at a certain time. This water originated in and

570   was in equilibrium with the leucite-tephritic country rock, where leucite served as a source for

571   potassium. A potassium source in the phonolite itself can be excluded due to the fresh appearance

572   of K-bearing phases, i.e. feldspars.

25

Revision 1

573   The Fohberg and Endhalden phonolites are both characterized by the occurrence of large

574   quantities of Ca-Na and Na species, showing the general trend from Ca-Na to Na-endmember

575   zeolite species. Although, the bulk rock composition and primary mineral chemistry of the

576   Fohberg and Endhalden phonolites are nearly identical (Spürgin et al. 2014, Fig. 2), the alteration

577   mineralogy yields significant differences by the appearance of analcime in the Endhalden

578   phonolite. This indicates that the hydrothermal systems evolved under different conditions during

579   their final stages. Nevertheless, both hydrothermal systems are characterized by a general closed

580   system behavior, whereas the change in mineralogy reflects continuing fluid-rock interaction

581   (Fig. 8) characterized by Ca-depletion and Na-enrichment, as well as an increase in Si/Al of the

582   zeolite species with time (Fig. 3).

583   Figure 8 illustrates the change in fluid composition during hydrothermal replacement as

584   function of aqueous silica activity and H_2O, respectively, and allows an estimation at fixed

585   pressure and temperature. The calculated quartz saturation plots at higher silica activities than the

586   observed phase equilibrium that buffers the activities of water and silica. This is in agreement

587   with the absence of quartz in the alteration assemblages. At a sub-solidus temperature of 250°C,

588   nepheline and albite buffer log $aSiO_{2,aq}$ to equilibrium values of -4 to -3 and at $aH_2O = 0.5$,

589   analcime is the only stable zeolite species. With decreasing temperatures to 150°C, natrolite

590   becomes stable at the expense of nepheline at the lower log $aSiO_{2,aq}$ limit of the analcime stability

591   field. At low-temperature conditions (50°C), natrolite is the dominant zeolite species, whereas the

592   aH_2O limit for natrolite stability decreases (Fig. 8). However, the textural relation indicates

593   unambiguously that analcime is formed after natrolite. This indicates that the change from

594   natrolite to analcime is either caused by an increase in temperature, or by an increase in SiO_2

595   activity (Fig. 8). An increase in temperature is rather implausible in the observed geological

596   context. Alternatively, an increase of SiO_2 activity is achieved by the total breakdown of

26

Revision 1

597   wollastonite, in contrast to the Fohberg phonolite, releasing SiO_2 to the fluid phase and Ca is

598   trapped in calcite. However, the appearance of analcime is not pervasive and therefore the

599   increase in SiO_2 activity seems to be more a local affect.

600   The cooling sequence natrolite-analcime is also known from other alkaline complexes, e.g.

601   Mont St. Hilaire, Canada (Schilling et al. 2011) or Norra Kärr, Sweden (Atanasova et al. 2017),

602   whereas in the Sushina Hill syenite, India (Chakrabarty et al. 2016), analcime formed at higher

603   temperatures than associated natrolite.

604

605

606   **IMPLICATIONS**

607

608   Minerals of the zeolite group form the major secondary replacement products in

609   holocrystalline, subvolcanic phonolites of the KVC. Zeolites are formed by the strongly selective

610   decay of primary feldspathoid minerals, that is evident from pseudomorphic replacement textures

611   and that is also known from other sites, e.g. from Tamazeght, Morocco, where gonnardite grows

612   at the expense of nepheline, sodalite and cancrinite due to late-stage reaction with meteoric

613   waters (Salvi et al. 2000; Schilling et al. 2009), from Mont St. Hilaire, Canada, where natrolite

614   and analcime grow along cracks and progressively replace sodalite (Schilling et al. 2011), and

615   from the Sushina Hill Complex, India, where nepheline, sodalite (and albite) decompose to

616   natrolite and analcime (Chakrabarty et al. 2016).

617   Several controlling factors are needed to 'zeolitize' such rocks, which include favorable

618   protolith mineralogy (e.g. feldspathoid minerals), the presence of a hydrothermal fluid with a

619   promoting chemical composition (e.g. elevated pH), fluid accessibility to the rock (e.g. porosity,

620   fracturing), and a p-T-environment which stabilizes zeolite minerals. As a consequence, the

27

621   geological setting is an important feature and may explain if an alkaline intrusive rock remains

622   unaltered, or becomes partially or fully zeolitized. Weisenberger et al. (2014) have shown that

623   fluid supply from the surrounding sedimentary rock sequence is an important factor for the

624   intense and pervasive zeolite formation in the Fohberg phonolite. It is presumed that a local

625   hydrothermal system was established, driven by the residual heat of the cooling intrusion, and

626   mineral decomposition led to *in situ* or local replacement by zeolites, both in the rock matrix and

627   in fissures. The same genetic model is applicable to the Endhalden phonolite, which is emplaced

628   in the same geologic setting of the eastern KVC. The major difference between these two and the

629   Kirchberg phonolite in the western KVC is found in the nature of the country rock. It is a water-

630   bearing sedimentary sequence in the eastern localities, probably below the paleo-groundwater

631   table, and a subaerial pyroclastic unit in the western locality (Kirchberg), which was probably

632   relatively dry due to its high porosity and the higher topographic position in the volcanic edifice

633   (Fig 8).

634   In a general view, two temporal scenarios are capable of leading to the zeolitization of such

635   intrusive rocks: I) Zeolite formation in a continuously cooling regime, i.e. in the postmagmatic

636   subsolidus stage after rock emplacement, which is characterized by the development of a

637   hydrothermal system. II) Zeolite formation temporally unrelated to rock intrusion due to re-

638   heating and re-emerging fluid activity, e.g. mineral formation in the waning stage of postdating

639   regional metamorphism of an alkaline intrusive rock. Examples include Norra Kärr, Sweden

640   (Atanasova et al. 2017), and Sushina Hill, India (Chakrabarty et al. 2016). Scenario I is the likely

641   scenario for zeolitization of all KVC phonolites, which show no evidence of re-heating and

642   reactivation of hydrothermal activity.

643   It is a noteworthy observation that these low-temperature secondary replacement reactions

644   are capable of generating zeolite deposits of economic interest. In the example shown in this

28

Revision 1

645   study, grades (total amount of zeolites, Table 2) of approximately 45 percent are achieved by

646   total decomposition of igneous minerals mentioned above. Although not of such high grade as

647   deposits formed by the crystallization of glass shards in uniform vitreous pyroclastic rocks,

648   zeolite deposits in subvolcanic to plutonic SiO_2-deficient alkaline rocks are nevertheless suitable

649   for a number of technical applications and should be considered as potentially valuable

650   lithologies.

651   Despite their use as cation exchangers, natural zeolites show various other technical

652   applications. One application is the production of blended cements, where zeolites serve as

653   supplementary cementitious material (SCM) due to their pozzolanic reactivity (Snellings et al.

654   2012). The use of SCM becomes increasingly important as it reduces the need of ordinary

655   Portland cement (OPC), and blended cements with a lower clinker ratio and higher SCM contents

656   are commonly produced worldwide, instead of OPC. Therefore, because SCM have the potential

657   to substitute a certain amount of OPC, they account for a significant reduction of the CO_2 release

658   during cement production, which is the third-largest source of anthropogenic CO_2 emissions

659   (Andrew 2018).

660   Previous studies have shown that the pozzolanic reactivity of a rock used as SCM is

661   dependent on a variety of controlling factors, including the specific mineralogical phase

662   assemblage of the rock, the grain sizes of the reactive phases as well as their behavior during

663   industrial processing, e.g. grinding and thermal treatment. The combination of these factors

664   complicates the comparison of different occurrences and the prediction of the reactivity (Mertens

665   et al. 2009; Snellings et al. 2010a,b; Özen et al. 2016). It is evident that each KVC phonolite, but

666   also each occurrence worldwide, has to be evaluated independently for its potential use as SCM,

667   if the general mineralogical characteristics are promising.

668

Revision 1

680

REFERENCES CITED

682 Albrecht, A. (1981) Mineralogische Untersuchungen des Phonoliths vom Fohberg, Kaiserstuhl,

683   mit besonderer Berücksichtigung der mafischen und akzessorischen Minerale. Diploma

684   Thesis, 146 p. Albert-Ludwigs-Universtity Freiburg.

685 Al Dwairi, R.A., Ibrahim, K.M., and Khoury, H.N. (2014) Potential use of faujasite-phillipsite

686   and phillipsite-chabazite tuff in purification of treated effluent from domestic wastewater

687   treatment plants. Environmental Earth Sciences, 71, 5071-5078.

688 Andrew, R.M. (2018) Global CO_2 emissions from cement production. Earth System Science

689   Data, 10, 195-217.

690 Atanasova, P., Marks, M.A.W., Heinig, T., Krause, J., Gutzmer, J., and Markl, G. (2017)

691   Distinguishing magmatic and metamorphic processes in peralkaline rocks of the Norra Kärr

30

Revision 1

692   Complex (southern Sweden) using textural and compositional variations of clinopyroxene

693   and eudialyte-group minerals. Journal of Petrology, 58, 361-384.

694   Baerlocher, C., McCusker, L.B., and Olson, D.H. (2007) Atlas of zeolite framework types, 398 p.

695   Amsterdam, Elsevier.

696   Baranyi, I., Lippolt, H.J., and Todt, W. (1976) Kalium-Argon-Altersbestimmungen an tertiären

697   Vulkaniten des Oberrheingraben-Gebiets II. Die Alterstraverse vom Hegau nach Lothringen.

698   Oberrheinische Geologische Abhandlungen, 25, 41-62.

699   Barth-Wirsching, U., and Höller, H. (1989) Experimental studies on zeolite formation conditions.

700   European Journal of Mineralogy, 1, 489-506.

701   Bernhard, F., and Barth-Wirsching, U. (2002) Zeolitization of a phonolitic ash flow by

702   groundwater in the Laacher See volcanic area, Eifel, Germany. Clays and Clay Minerals, 50,

703   710-725.

704   Braunger, S., Marks, M.A.W., Walter, B.F., Neubauer, R., Reich, R., Wenzel, T., Parsapoor, A.,

705   and Markl, G. (2018) The petrology of the Kaiserstuhl Volcanic Complex, SW Germany: the

706   importance of metasomatized and oxidized lithospheric mantle for carbonatite generation.

707   Journal of Petrology, 59, 1731-1762.

708   Cappelletti, P., Petrosino, P., de Gennaro, M., Colella, A., Graziano, S.F., D'Amore, M.,

709   Mercurio, M., Cerri, G., de Gennaro, R., Rapisardo, G., and Langella, A. (2015) The "Tufo

710   Giallo della Via Tiberina" (Sabatini Volcanic District, Central Italy): a complex system of

711   lithification in a pyroclastic current deposit. Mineralogy and Petrology, 109, 85-101.

712   Chakrabarty, A., Mitchell, R., Ren, M., Saha, P., Pal, S., Pruseth, K., and Sen, A. (2016)

713   Magmatic, hydrothermal and subsolidus evolution of the agpaitic nepheline syenites of the

714   Sushina Hill Complex, India: implications for the metamorphism of peralkaline syenites.

715   Mineralogical Magazine, 80, 1161-1193.

Revision 1

716   Cheary, R.W., and Coelho, A. (1992) A fundamental parameters approach to X-ray line-profile

717   fitting. Journal of Applied Crystallography, 25, 109-121.

718   Çiftçi, E., Hogan, J.P., Kolayli, H., and Çadirli, E. (2008) Natrolitite, an unusual rock –

719   occurrence and petrographic and geochemical characteristics (eastern Turkey). Clays and

720   Clay Minerals, 56, 207-221.

721   Cochemé, J.J., Lassauvagerie, A.C., Gonzalez-Sandoval, J., Perez-Segura, E., and Münch, P.

722   (1996) Characterisation and potential economic interest of authigenic zeolites in continental

723   sediments from NW Mexico. Mineralium Deposita, 31, 482-491.

724   Coombs, D.S., Alberti, A., Artioli, A., Armbruster, T., Colella, C., Galli, E., Grice, J.D., Liebau,

725   F., Mandarino, J.A., Minato, H., Nickel, E.H., Passaglia, E., Peacor, D.R., Quartieri, S.,

726   Rinaldi, R., Ross, M., Sheppard, R.A., Tillmanns, E., and Vezzalini, G. (1997)

727   Recommended nomenclature for zeolite minerals: report of the subcommittee on zeolites of

728   the international mineralogical association, commission on new minerals and mineral names:

729   Canadian Mineralogist, 35, 1571-1606.

730   Czygan, W. (1973) Götzenit, ein komplexes Ti-Zr-Silikat aus dem Kaiserstuhl. Berichte der

731   naturforschenden Gesellschaft zu Freiburg i.Br., 63, 5-12.

732   Czygan, W. (1977) Petrographie und Geochemie der Foidsyenit-Einschlüsse im Phonolith von

733   Niederrotweil im Kaiserstuhl. Berichte der naturforschenden Gesellschaft zu Freiburg i.Br.,

734   67, 41-52.

735   Deer, W.A., Howie, R.A., Wise. W.S., and Zussman, J. (2004) Framework silicates:silica

736   minerals, feldspathoids and the zeolites. The Geological Society of London, London.

737   de'Gennaro, M., and Langella, A. (1996) Italian zeolitized rocks of technological interest.

738   Mineralium Deposita, 31, 452-472.

32

Revision 1

739 de'Gennaro, M., Cappelletti, P., Langella, A., Perrotta, A., and Scarpati, C. (2000) Genesis of

740   zeolites in the Neapolitan Yellow Tuff: geological, volcanological and mineralogical

741   evidence. Contributions to Mineraloggy and Petrolgy, 139, 17-35.

742 Eggleton, R.A., and Keller, J. (1982) The palagonitization of limburgitic glass – a TEM study.

743   Neues Jahrbuch für Mineralogie, Monatsheft, 321-336.

744 Faccini, B., Di Giuseppe, D., Malferrari, D., Coltorti, M., Abbondanzi, F., Campisi, T., Laurora,

745   A., and Passaglia, E. (2015) Ammonium-exchanged zeolitite preparation for agricultural

746   uses: from laboratory tests to large-scale application in ZeoLIFE project prototype. Periodico

747   di Mineralogia, 84, 303-321.

748 Harada, K., and Nagashima, K. (1972) New data on the analcime-wairakite series. American

749   Mineralogist, 57, 924-931.

750 Hay, R.L., and Sheppard, R.A. (2001) Occurrence of Zeolites in Sedimentary Rocks: An

751   Overview. Reviews in Mineralogy and Geochemistry, 45, 217-234.

752 Helgeson, H.C., Delany, J.M., Nesbitt, H.W., and Bird, D.K. (1978) Summary and critique of the

753   thermodynamic properties of rock-forming minerals. American Journal of Science, 278-A,

754   1–229.

755 Ibrahim, K.M., and Hall, A. (1996) The authigenic zeolites of the Aritayn volcanoclastic

756   formation, north-east Jordan. Mineralium Deposita, 31, 514-522.

757 Ibrahim, K.M. (2004) Mineralogy and chemistry of natrolite from Jordan. Clay Minerals, 39, 47-

758   55.

759 Ibrahim, K.M., Khoury, H.N., and Tuffaha, R. (2016) Mo and Ni removal from drinking water

760   using zeolitic tuff from Jordan. Minerals, 6, 1-13.

Revision 1

761 Izzo, F., Grifa, C., Germinario, C., Mercurio, M., De Bonis, A., Tomay, L., and Langella, A.

762   (2018) Production technology of mortar-based building materials from the Arch of Trajan

763   and the Roman Theatre in Benevento, Italy. The European Physical Journal Plus, 133, 363.

764 Jackson, M.D., Mulcahy, S.R., Chen, H., Li, Y., Li, Q., Cappelletti, P., and Wenk, H.R. (2017)

765   Phillipsite and Al-tobermorite mineral cements produced through low-temperature water-

766   rock reactions in Roman marine concrete. American Mineralogist, 102, 1435-1450.

767 Johnson, J.W., Oelkers, E.H., and Helgeson, H.C. (1992) SUPCRT92: A software package for

768   calculating the standard molal thermodynamic properties of minerals, gases, aqueous species,

769   and reactions from 1 to 5000 bar and 0 to 1000°C. Computers and Geosciences, 18, 899-947.

770 Kalló, D. (2001) Applications of natural zeolites in water and wastewater treatment. Reviews in

771   Mineralogy and Geochemistry, 45, 519-550.

772 Kassautzki, M. (1983) Phonolith als puzzolanischer Zumahlstoff in der Zementindustrie. Zement-

773   Kalk-Gips International, 36, 688-692.

774 Keller, J. (1964) Zur Vulkanologie des Burkheim-Sponeck Gebietes im westlichen Kaiserstuhl.

775   Berichte der naturforschenden Gesellschaft zu Freiburg i. Br., 54, 107-130.

776 Keller, J. (2001) Kaiserstuhl alkaline rock-carbonatitic complex - Excursion notes. ESF

777   Carbonatite Workshop, Breisach.

778 Keller, J., Sigmund, J., and Müller-Sigmund, H. (1997) Mantle xenoliths in Rhinegraben

779   volcanics from the Black Forest-Vosges Dome. Terra Nova, 9, Supplement 1, 56.

780 Kónya, P., and Szakáll, S. (2011) Occurrence, composition and paragenesis of the zeolites and

781   associated minerals in the alkaline basalt of a maar-type volcano at Haláp Hill, Balaton

782   Highland, Hungary. Mineralogical Magazine, 75, 2869-2885.

783 Kousehlar, M., Weisenberger, T.B., Tutti, F., and Mirnejad, H. (2012) Fluid control on low-

784   temperature mineral formation in volcanic rocks of Kahrizak, Iran. Geofluids, 12, 295-311.

Revision 1

785   Kraml, M., Pik, R., Rahn, M., Selbekk, R.S., Carignan, J., and Keller, J. (2006) A new multi-

786   mineral age reference material for $^{40}Ar/^{39}Ar$, (U/Th)/He and fission track dating methods:

787   The Limberg t3 tuff. Geostandards and Geoanalytical Research, 30, 73-86.

788   Langella, A., Bish, D.L., Cappelletti, P., Cerri, G, Colella, A., de Gennaro, R., Graziano, S.F.,

789   Perrotta, A., Scarpati, C., and de Gennaro, M. (2013) New insights into the mineralogical

790   facies distribution of Campanian Ignimbrite, a relevant Italian industrial material. Applied

791   Clay Science, 72, 55-73.

792   Leggo, P.J., and Ledésert, B. (2001) Use of organo-zeolitic fertilizer to sustain plant growth and

793   stabilize metallurgical and mine-waste sites. Mineralogical Magazine, 65, 563-570.

794   Leggo, P.J., Ledésert, B., and Day, J. (2010) Organo-zeolitic treatment of mine waste to enhance

795   the growth of vegetation. European Journal of Mineralogy, 22, 813-822.

796   Loewenstein, W. (1954) The distribution of aluminum in the tetrahedra of silicates and

797   aluminates: American Mineralogist, 39, 92-96.

798   Madsen, I.C., and Scarlett, N.V.Y. (2008) Quantitative phase analysis. In R.E. Dinnebier and

799   S.J.L. Billinge, Eds., Powder diffraction: theory and practice, p. 298-331. RSC Publishing,

800   Cambridge, U.K.

801   Marzi, E. (1983) Die Mineralien des Fohbergs bei Bötzingen (Oberschaffhausen) im Kaiserstuhl.

802   Der Aufschluss, 34, 205-214.

803   Marzi, E., and Spürgin, S. (2017) Neufund im klassischen Vulkangebiet – Merlinoit aus dem

804   Kaiserstuhl. Lapis 5/2017, 12-23.

805   Mercurio, M., Mercurio, V., de Gennaro, B., de Gennaro, M., Grifa, C., Langella, A., and Morra,

806   V. (2010) Natural zeolites and white wines from Campania region (Southern Italy): a new

807   contribution for solving some oenological problems. Periodico di Mineralogia, 79, 95-112.

Revision 1

808 Mercurio, M., Cappelletti, P., de Gennaro, B., de Gennaro, M., Bovera, F., Iannaccone, F., Grifa,

809   C., Langella, A., Monetti, V., and Esposito, L. (2016) The effect of digestive activity of pig

810   gastro-intestinal tract on zeolite-rich rocks: An in vitro study. Microporous and Mesoporous

811   Materials, 225, 133-136.

812 Mercurio, M., Izzo, F., Langella, A., Grifa, C., Germinario, C., Daković, A., Aprea, P., Pasquino,

813   R., Cappelletti, P., Graziano, F.S., and De Gennaro, B. (2018) Surface-modified phillipsite-

814   rich tuff from the Campania region (southern Italy) as a promising drug carrier: An ibuprofen

815   sodium salt trial. American Mineralogist, 103, 700-710.

816 Mertens, G., Snellings, R., Van Balen, K., Bicer-Simsir, B., Verlooy, P., and Elsen, J. (2009)

817   Pozzolanic reactions of common natural zeolites with lime and parameters affecting their

818   reactivity. Cement and Concrete Research, 39, 233-240.

819 Napia, C., Sinsiri, T., Jaturapitakkul, C., and Chindaprasirt, P. (2012) Leaching of heavy metals

820   from solidified waste using portland cement and zeolite as a binder. Waste Management, 32,

821   1459-1467.

822 Neuhoff, P.S. (2000) Thermodynamic properties and parageneses of rock-forming zeolites. Ph.D.

823   thesis, p. 240. Stanford University, Stanford, CA.

824 Neuhoff, P.S., Fridriksson, T. Arnorsson, S., and Bird, D.K. (1999) Porosity evolution and

825   mineral paragenesis during low-grade metamorphism of basaltic lavas at Teigarhorn, eastern

826   Iceland. American Journal of Science, 299, 467-501.

827 Neuhoff, P.S., Rogers, K.L., Stannius, L.S., Bird, D.K., and Pedersen, A.K. (2006) Regional very

828   low-grade metamorphism of basaltic lavas, Disko-Nuussuaq region, West Greenland. Lithos,

829   92, 33-54.

830 Özen, S., Göncüoğlu, M.C., Liguori, B., de Gennaro, B., Cappelletti, P., Gatta, G.D, Iucolano, F,

831   and Colella, C. (2016) A comprehensive evaluation of sedimentary zeolites from Turkey as

36

Revision 1

832   pozzolanic addition of cement- and lime-based binders. Construction and Building Materials,

833   105, 46-61.

834 Passaglia, E. (1970) The crystal chemistry of chabazite. American Mineralogist, 55, 1278-1301.

835 Rodriguez-Navarro, C., Ruiz-Agudo, E., Luque, A., Rodriguez-Navarro, A.B., and Ortega-

836   Huertas, M. (2009) Thermal decomposition of calcite: Mechanisms of formation and textural

837   evolution of CaO nanocrystals. American Mineralogist, 94, 578-593.

838 Rogers, K.L., Neuhoff, P.S., Pedersen, A.K., and Bird, D.K. (2006) CO_2 metasomatism in a

839   basalt-hosted petroleum reservoir, Nuussuaq, West Greenland. Lithos, 92, 55-82.

840 Salvi, S., Fontan, F., Monchoux, P., Williams-Jones, A.E., and Moine, B. (2000) Hydrothermal

841   mobilization of high field strength elements in alkaline igneous systems: evidence from the

842   Tamazeght complex (Morocco). Economic Geology, 95, 559-576.

843 Schilling, J., Marks, M.A.W., Wenzel, T., and Markl, G. (2009) Reconstruction of magmatic to

844   subsolidus processes in an agpaitic system using eudialyte textures and composition: a case

845   study from Tamazeght, Morocco. Canadian Mineralogist, 47, 351-365.

846 Schilling, J., Marks, M.A.W., Wenzel, T., Vennemann, T., Horváth, L., Tarassoff, P., Jacob,

847   D.E., and Markl, G. (2011) The magmatic to hydrothermal evolution of the intrusive Mont

848   Saint-Hilaire Complex: insights into the late-stage evolution of peralkaline rocks. Journal of

849   Petrology, 52, 2147-2185.

850 Snellings, R., Mertens, G., Gasharova, B., Garbev, K., and Elsen, J. (2010a) The pozzolanic

851   reaction between clinoptilolite and portlandite: a time and spatially resolved IR study.

852   European Journal of Mineralogy, 22, 767-777.

853 Snellings, R., Mertens, G., and Elsen, J. (2010b) Calorimetric evolution of the early pozzolanic

854   reaction of natural zeolites. Journal of Thermal Analysis and Calorimetry, 101, 97-105.

Revision 1

855   Snellings, R., Mertens, G., and Elsen, J. (2012) Supplementary cementitious materials. Reviews

856   in Mineralogy and Geochemistry, 74, 211-278.

857   Spürgin, S., Weisenberger, T., and Hörth, J. (2008) Das Leucitophyrvorkommen vom

858   Strümpfekopf im Kaiserstuhl – eine historische und mineralogische Betrachtung. Berichte

859   der naturforschenden Gesellschaft zu Freiburg i.Br., 98, 221-244.

860   Spürgin, S., Weisenberger, T., Rosing-Schow, N., and Vasilopoulos, M. (2014) Phonolite-hosted

861   zeolite deposits in the Kaiserstuhl Volcanic Complex, Germany. Zeolites 2014 Book of

862   Abstracts, Belgrade, 221-222.

863   Tschernich, R.W. (1992) Zeolites of the world, 563 p. Geoscience Press, Phoenix.

864   van Reeuwijk, L.P. (1972) High-temperature phases of zeolites of the natrolite group. American

865   Mineralogist,57, 499-510.

866   Wedepohl, K.H., Gohn, E., and Hartmann, G. (1994) Cenozoic alkali basaltic magmas of western

867   Germany and their products of differentiation. Contributions to Mineralogy and Petrology,

868   115, 253-278.

869   Weisenberger, T., and Selbekk, R.S. (2009) Multi-stage zeolite facies mineralization in the

870   Hvalfjördur area, Iceland. International Journal of Earth Sciences, 98, 985-999.

871   Weisenberger, T., and Spürgin, S. (2009) Zeolites in alkaline rocks of the Kaiserstuhl Volcanic

872   Complex - new microprobe investigation and their relationship to the host rock. Geologica

873   Belgica, 12, 75-91.

874   Weisenberger, T.B., Spürgin, S., and Lahaye, Y. (2014) Hydrothermal alteration and zeolitization

875   of the Fohberg phonolite, Kaiserstuhl Volcanic Complex, Germany. International Journal of

876   Earth Sciences, 103, 2273-2300.

877   Whitney, D.L., and Evans, B.W. (2010) Abbreviations for names of rock-forming minerals.

878   American Mineralogist, 95, 185-187.

Revision 1

879   Wilson, M., and Downes, H. (1991) Tertiary – Quaternary extension-related alkaline magmatism

880   in western and central Europe. Journal of Petrology, 32, 811-849.

881   Wimmenauer, W. (1962) Beiträge zur Petrographie des Kaiserstuhls. Teil IV: Die Gesteine der

882   phonolitischen Familie. Teil V: Die subvulkanischen Breccien. Neues Jahrbuch für

883   Mineralogie Abhandlungen, 98, 367-415.

884   Wimmenauer, W. (1974) The alkaline province of central Europe and France. In H. Sorensen,

885   Ed., The alkaline rocks, p. 286-291. Wiley, London.

886   Wimmenauer, W. (2003) Geologische Karte von Baden-Württemberg 1:25000, Kaiserstuhl.

887   Landesamt für Geologie, Rohstoffe und Bergbau Baden-Württemberg, Freiburg.

888   Wimmenauer, W. (2010) Kalkadern in vulkanischen und Sedimentgesteinen des Kaiserstuhls.

889   Mitteilungen des badischen Landesvereins für Naturkunde und Naturschutz, 21, 49-67.

890

39

Revision 1

891   FIGURE 1. a) Geological map of the Kaiserstuhl Volcanic Complex (KVC), showing the

892   investigated subvolcanic phonolite intrusions, b) Map of Germany with location of the KVC.

893

894   FIGURE 2. Representative thin section microphotographs and BSE images of phonolites

895   from the KVC, a,b) Wollastonite bearing, slightly porphyritic phonolite from Fohberg. The

896   phonolite shows pseudomorphic replacement of feldspathoid minerals by various zeolites. Barite

897   is present as small inclusions in zeolite aggregates, c,d) Endhalden phonolite with similar igneous

898   textures as Fohberg phonolite. In addition, analcime is present as secondary mineral, e,f)

899   Kirchberg phonolite showing primary fresh feldspathoid minerals, as well as an example of a

900   zeolite alteration sequence. Mineral abbreviations: Adr andradite, Agt aegirine-augite, Anl

901   analcime, Brt barite, Cal calcite, Cbz chabazite, Gon gonnardite, Hyn haüyne, Kfs alkali feldspar,

902   Pl plagioclase, Thm thomsonite, Wo wollastonite.

903

904   FIGURE 3. Chemical characterization of zeolites from phonolites of the KVC, showing

905   variations in extra-framework cations and T_{Si} = Si/Al variations in the Si-R^{2+}-R^+ plot. The dashed

906   areas represent compositional variation for particular zeolite species (adapted from Deer et al.

907   2004).

908

909   FIGURE 4. Thermal behavior of phonolites a) Endhalden, b) Fohberg, c) Kirchberg. Major

910   weight loss in a) and endothermal peaks in b) correspond to H_2O loss of zeolites and CO_2 loss of

911   calcite.

912

913   FIGURE 5. Chemical composition and classification of sodalite-group minerals from the

914   Kirchberg phonolite.

40

Revision 1

915

916   FIGURE 6. Geological sketch section showing the setting of phonolites in the western (left)

917   and eastern (right) Kaiserstuhl. Dashed line represents the present erosional level. Triangular

918   diagrams show the temporal succession of zeolite formation (for full labeling see Fig. 3). The

919   Kirchberg phonolite is a shallow intrusion into relatively dry subaerial lavas and pyroclastites.

920   After an initial closed-system evolution (1) limited influx of K-rich water from leucite-tephritic

921   country rock led to formation of chabazite (2). The Fohberg and Endhalden phonolites were

922   emplaced into a pre-volcanic sedimentary sequence and experienced influx of formation water

923   during cooling, which established a hydrothermal system and continuous, pervasive closed-

924   system zeolite formation (3).

925

926   FIGURE 7. Calculated mineral stability diagram between 50 and 100 °C at a constant

927   pressure of 10 MPa as a function of cation activity ratios in the Al_2O_3–Na_2O– CaO–SiO_2–H_2O

928   system. The diagram assumes aluminum balance and quartz undersaturation (a(Qz) = 0.95) and

929   a(H_2O) = 1. Mineral abbreviations: Cbz chabazite, Grs grossular, Kln kaolinite, Mes mesolite,

930   Ntr natrolite, Thm thomsonite, Wo wollastonite.

931

932   FIGURE 8. Quantitative $aSiO_2$–aH_2O diagrams for selected Na–Al silicates at constant

933   pressure (10 MPa) within the temperature range from 50 to 250 °C. Dashed lines represent the

934   lower limits of quartz saturation at 50°C. Mineral abbreviations: Ab albite, Anl analcime, Ne

935   nepheline, Ntr natrolite, Qz quartz.
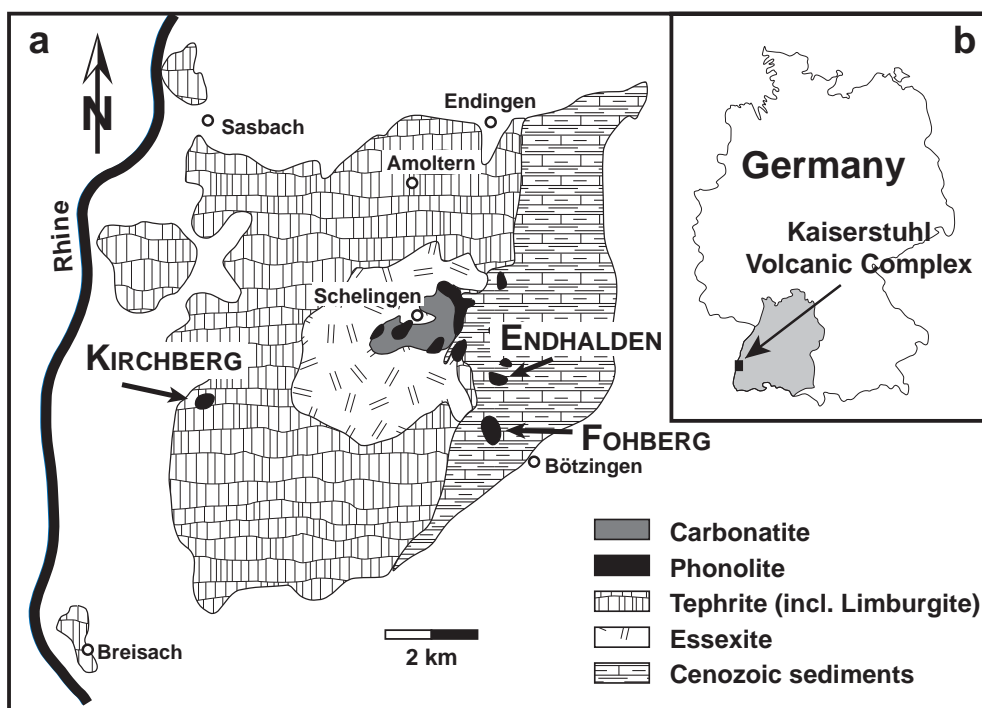
936

937

41

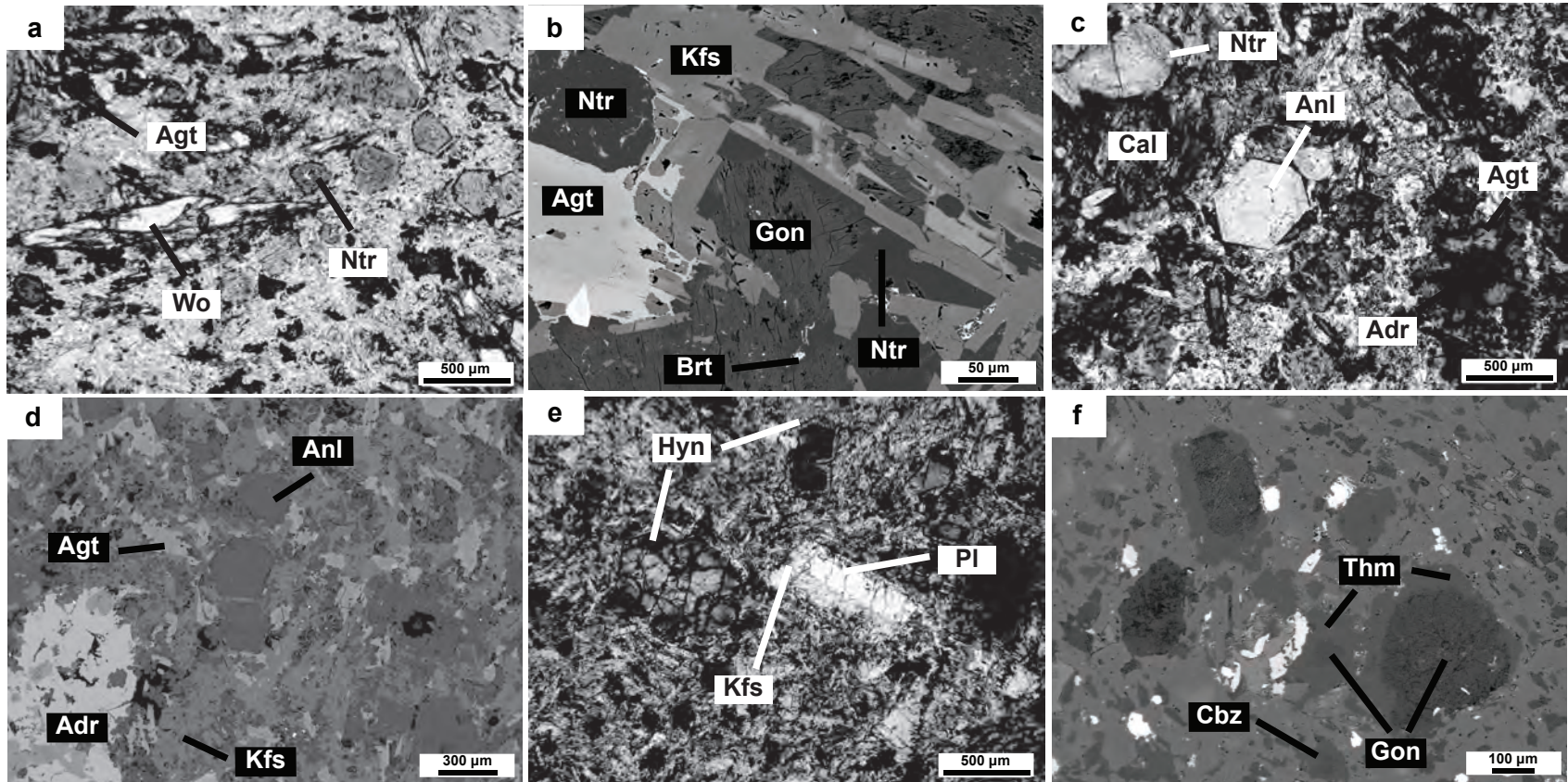Figure: 1, width: 1 columns (3 inches)

Figure: 2, width: 2 columns (6.5 inches)

Figure: 3, width: 1 column (3 inches)

Figure: 4, width: 2 columns (6.5 inches)

K$_2$O

Haüyne

Nosean

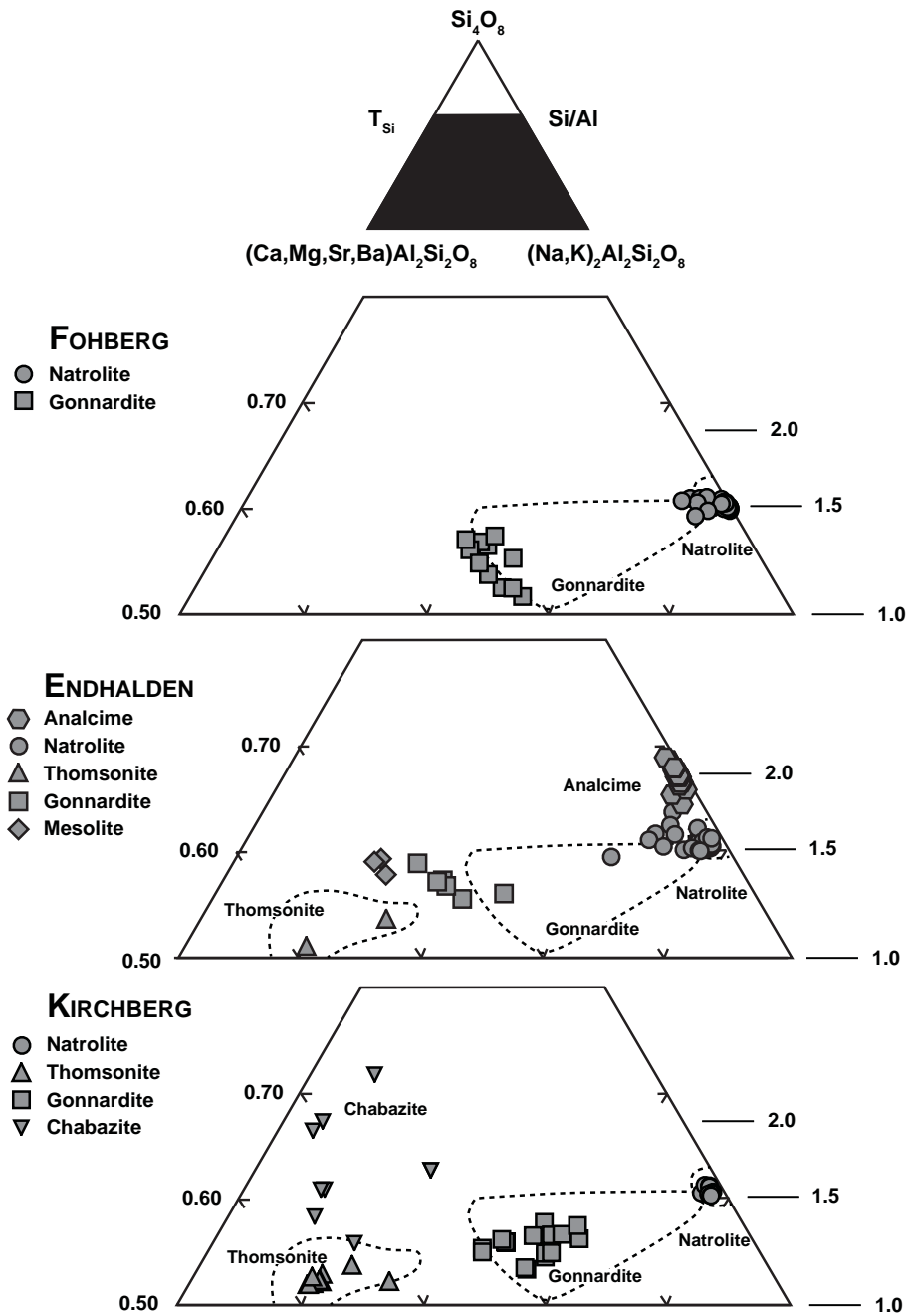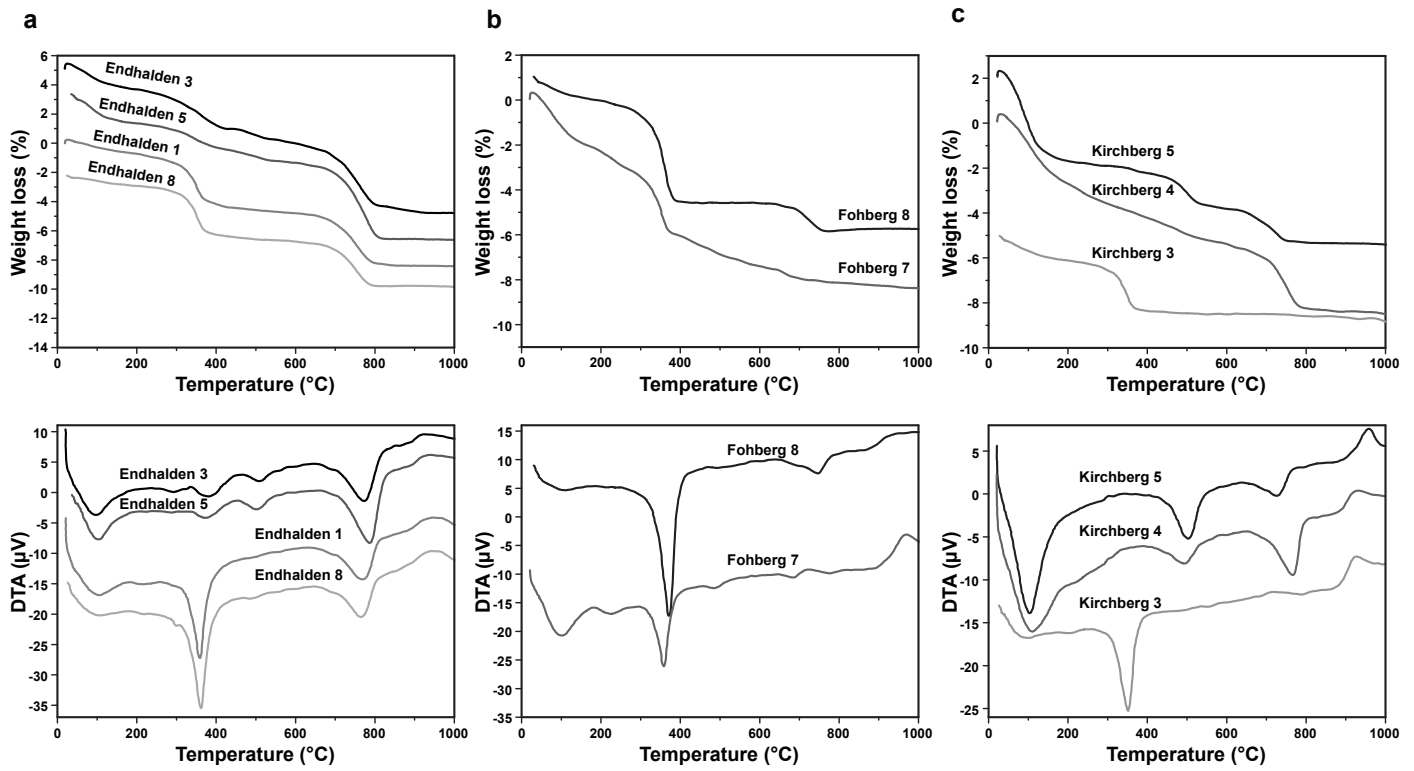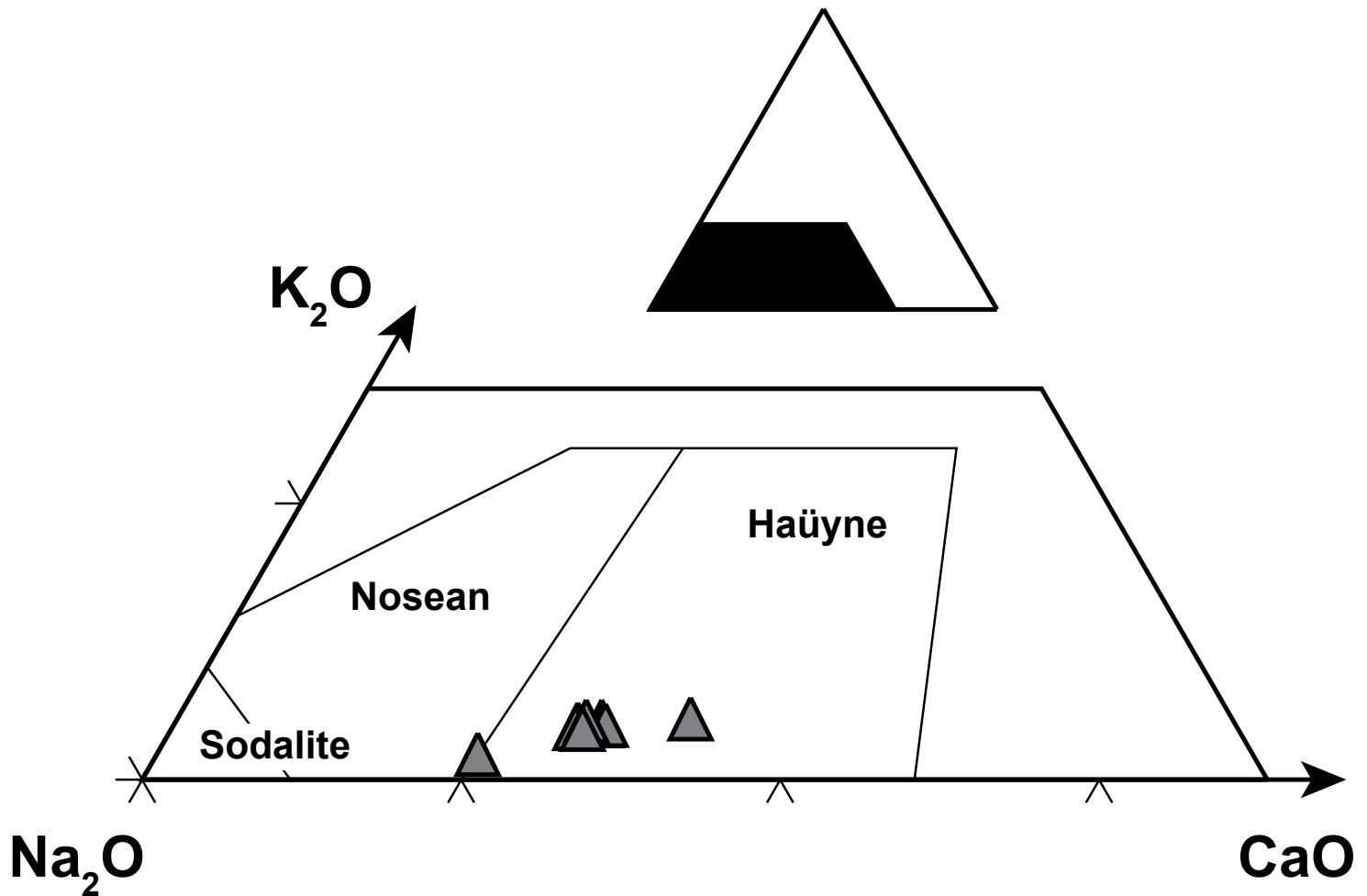**Sodalite**

Na$_2$O

CaO

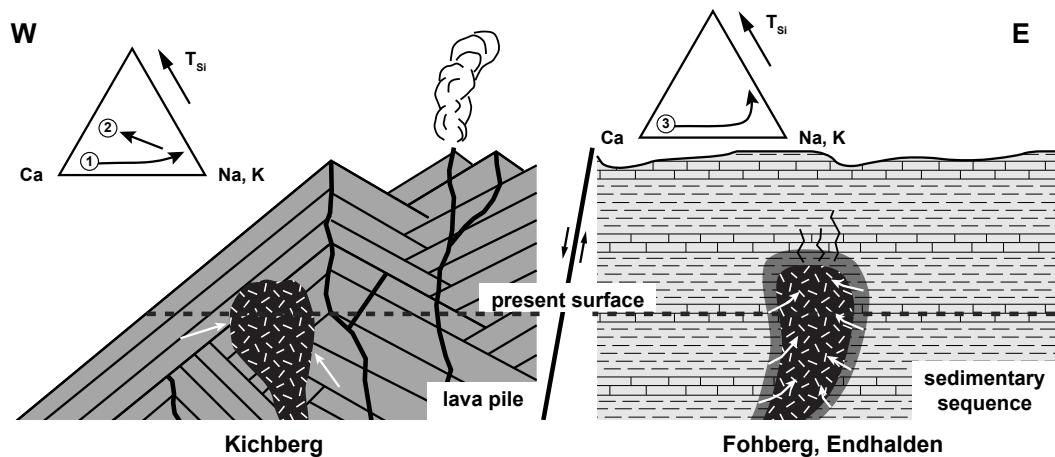Figure: 5, width: 1 column (3 inches)
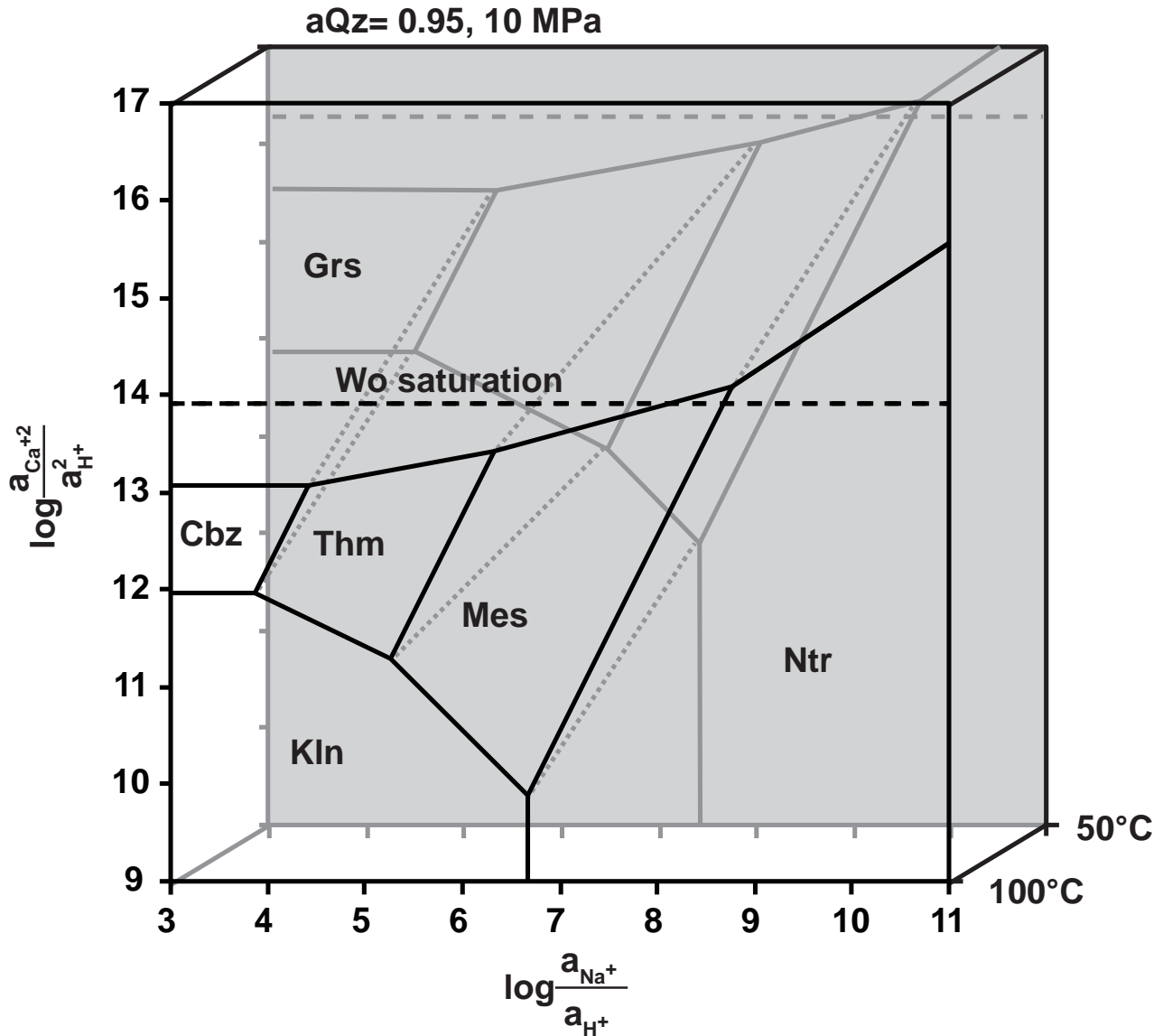
Figure: 6, width: 2 columns (6.5 inches)

Figure: 7, width: 1 column (3 inches)

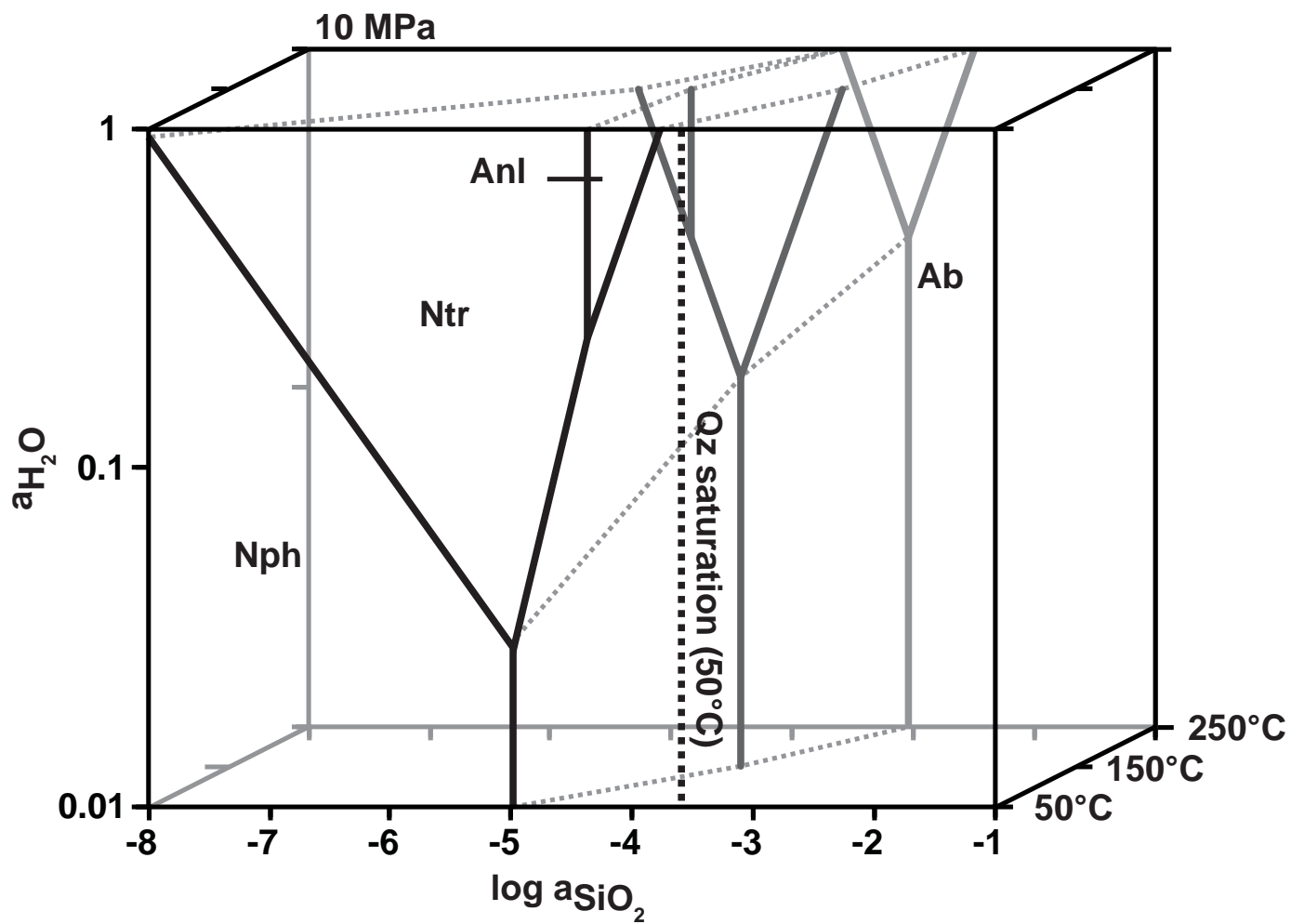Figure: 8, width: 1 column (3 inches)

TABLE 1. General petrographic characteristics of intrusive phonolite stocks in the KVC

Phonolite	Locality	Major primary minerals [a]	Secondary mineral assemblages [a]	Alteration style	Remarks
Endhalden	Bötzingen	Sa, (*FM?*), Aeg, Adr, (Wo)	Ntr, Anl, Gon, Cal, ±Thm, ±Mes, ±Clay minerals	vesicles, rock matrix	homogeneous secondary mineralization throughout phonolite body
Fohberg	Bötzingen	(*FM?*), Sa, Aeg, Wo/(Wo), Adr, ±Ttn	Ntr, Gon, Cal, ±Thm, ±Mes	fissures, rock matrix	homogeneous secondary mineralization throughout phonolite body
Kirchberg	Niederrotweil	Sa, Pl, Hyn/(Hyn), Aeg, Adr, Mag, ±Ttn	Cal, Cbz, Clay minerals Thm, Gon Ntr, Gon, Thm Cal, Cbz, Clay minerals Cbz, Clay minerals Clay minerals	fissures (partially), rock matrix (partially)	various assemblages; heterogeneous secondary mineralization throughout phonolite body

[a] Mineral abbreviations after Whitney and Evans (2010), except Gon = gonnardite; *FM?* = unidentified feldspathoid mineral (most likely a member of the sodalite group, see text). Aeg refers to aegirine-augite solid solution. Mineral abundances are noted on a qualitative basis. Mineral names in brackets: primary mineral decomposed and only recognized due to shape of pseudomorphic aggregates.

1

TABLE 2. Results of X-ray diffraction (XRD) and quantitative phase analyses (QPA) of phonolites in wt%

	Endhalden_1	Endhalden_3	Endhalden_5[d]	Endhalden_8	Fohberg_7	Fohberg_8	Kirchberg_3	Kirchberg_4	Kirchberg_5
Natrolite	26	2	1	37	20	40	15	-	-
Gonnardite	5	4	3	4	25	3	11	D [c]	-
Thomsonite	-	-	-	D	-	-	D	-	-
Analcime	6	17	14	7	-	-	-	-	-
Chabazite	-	-	-	-	-	-	-	1	1
Sanidine [a]	43	49	47	33	42	37	69	82	82
Plagioclase	-	-	-	-	-	-	-	4	D
Sodalite-Haüyne	-	-	-	-	-	-	-	D	D
Wollastonite	-	-	-	-	-	5	-	-	-
Aegirine-Augite	9	14	13	9	11	11	4	6	7
Andradite	2	1	2	2	1	1	1	2	6
Calcite	9	13	14	9	1	4	1	5	4
Clays	-	-	6	-	-	-	-	D	D
Zeolites (Ntr+Gon+Anl+Cbz) [b]	37	23	18	48	45	43	26	1	1
X_{Gon} = Gon/(Ntr+Gon+Anl) [b]	0.14	0.17	0.17	0.08	0.56	0.07	0.42	-	-
X_{Zeo} = Zeo/(Zeo+Fsp) [b]	0.46	0.32	0.28	0.59	0.52	0.54	0.27	0.01	0.01

[a] Best fit was achieved using a monoclinic sanidine structure model. However, the presence of minor amounts of alkali feldspar with a slightly deviating structure cannot be excluded.
[b] Mineral abbreviations after Whitney and Evans (2010), except Gon = gonnardite.
[c] D = detected and identified by powder XRD but not quantified by Rietveld QPA.
[d] Affected by surficial weathering

1

TABLE 3. Representative zeolite compositions of phonolites in the KVC in wt% and formula calculations

Location	Fohberg	Endhalden	Kirchberg	Endhalden	Fohberg	Endhalden	Kirchberg	Endhalden	Kirchberg	Kirchberg
Mineral	Natrolite	Natrolite	Natrolite	Analcime	Gonnardite	Gonnardite	Gonnardite	Thomsonite	Thomsonite	Chabazite
Analysis no	2-47	1-237	3-34	5-254	NBK-20	1-191	2-18	1-247	2-15	1-7
SiO_2	46.46	46.27	48.54	55.19	42.52	44.67	43.09	35.67	37.67	46.42
Al_2O_3	27.20	26.02	26.10	22.35	27.54	26.52	28.87	29.13	29.65	25.36
CaO	1.14	0.58	0.22	0.00	6.97	8.68	7.16	7.70	13.15	10.87
SrO	0.08	0.00	0.11	0.00	1.16	0.82	0.00	9.54	0.10	1.06
BaO							0.04		0.00	0.05
Na_2O	15.00	15.06	15.48	13.31	8.10	5.98	9.36	3.70	3.62	0.94
K_2O	0.07	0.04	0.00	0.01	0.04	0.03	0.02	0.00	0.01	2.22
Total[a]	89.95	87.97	90.45	90.86	86.32	86.69	88.55	85.74	84.20	86.91
O	80	80	80	96	80	80	80	80	80	24
Si	23.69	24.07	24.50	32.54	22.72	23.54	22.38	20.35	20.72	7.32
Al	16.35	15.95	15.71	15.54	17.34	16.47	17.68	19.59	19.22	4.71
Ca	0.62	0.32	0.12	0.00	3.99	4.90	3.99	4.71	7.75	1.83
Sr	0.02	0.00	0.03	0.00	0.36	0.25	0.00	3.16	0.03	0.10
Ba	0.00	0.00	0.00	0.00	0.00	0.00	0.01	0.00	0.00	0.00
Na	14.83	15.19	15.15	15.21	8.39	6.07	9.43	4.09	3.87	0.29
K	0.04	0.03	0.00	0.01	0.03	0.02	0.02	0.00	0.01	0.45
E%[b]	1.13	0.59	0.50	2.06	1.34	0.29	1.40	-1.14	-1.11	2.40
Si/(Si+Al)	0.59	0.60	0.61	0.68	0.57	0.59	0.56	0.51	0.52	0.61

[a] Analyses yield traces of Fe, Mg, Mn, Ti.
[b] E% = (100 × [Al − (Na + K) − 2(Ca + Sr + Ba)]/[(Na + K) + 2(Ca + Sr + Ba)]

1

TABLE 4. Representative haüyne compositions from the Kirchberg phonolite wt% and formula calculations

Analysis no.	4-60	4-59	4-58	4-57	4-26
SiO_2	36.23	35.23	35.54	35.61	34.11
TiO_2	0.00	0.00	0.02	0.00	0.00
Al_2O_3	28.78	27.71	28.14	28.08	27.39
Fe_2O_3	0.36	0.76	0.43	0.62	0.37
CaO	5.01	6.25	6.48	6.52	6.55
Na_2O	19.47	17.08	16.69	16.85	18.31
K_2O	0.49	0.88	0.94	1.00	1.00
SrO	0.00	0.05	0.00	0.03	0.00
SO_3	4.99	6.96	6.60	6.60	7.19
F	0.00	0.00	0.00	0.00	0.00
Cl	3.03	1.85	1.58	1.55	1.42
-O=Cl	0.68	0.42	0.36	0.35	0.32
Total[a]	97.70	96. 35	96.10	96.51	96.04
Numbers of ions on the basis of 21 (O) associated with $3Al_2O_3 \cdot 6SiO_2$					
Si	6.20	6.23	6.21	6.22	6.16
Al	5.80	5.77	5.79	5.78	5.84
$\sum T$	12.00	12.00	12.00	12.00	12.00
Ti	0.00	0.00	0.00	0.00	0.00
Fe^{3+}	0.02	0.05	0.03	0.04	0.03
Ca	0.92	1.18	1.21	1.22	1.27
Na	6.46	5.85	5.65	5.71	6.42
K	0.11	0.20	0.21	0.22	0.23
Sr	0.00	0.00	0.00	0.00	0.00
$\sum X$	7.51	7.29	7.11	7.19	7.94
F	0.00	0.00	0.00	0.00	0.00
SO_4	0.77	1.11	1.04	1.04	1.17
Cl	0.88	0.55	0.47	0.46	0.44
$\sum Z$	1.65	1.66	1.51	1.50	1.61

[a] Total includes traces of Mg, Mn, Zr.

1